

RS-8232-2/62328

SANDIA REPORT

SAND85-0708 • Unlimited Release • UC-35

C.1

Printed April 1985



8232-2/062328



00000001 -

SCAP – A Shaped Charge Analysis Program – User's Manual for SCAP 1.0

A. C. Robinson

Prepared by
Sandia National Laboratories
Albuquerque, New Mexico 87185 and Livermore, California 94550
for the United States Department of Energy
under Contract DE-AC04-76DP00789



Issued by Sandia National Laboratories, operated for the United States Department of Energy by Sandia Corporation.

NOTICE: This report was prepared as an account of work sponsored by an agency of the United States Government. Neither the United States Government nor any agency thereof, nor any of their employees, nor any of their contractors, subcontractors, or their employees, makes any warranty, express or implied, or assumes any legal liability or responsibility for the accuracy, completeness, or usefulness of any information, apparatus, product, or process disclosed, or represents that its use would not infringe privately owned rights. Reference herein to any specific commercial product, process, or service by trade name, trademark, manufacturer, or otherwise, does not necessarily constitute or imply its endorsement, recommendation, or favoring by the United States Government, any agency thereof or any of their contractors or subcontractors. The views and opinions expressed herein do not necessarily state or reflect those of the United States Government, any agency thereof or any of their contractors or subcontractors.

Printed in the United States of America
Available from
National Technical Information Service
U.S. Department of Commerce
5285 Port Royal Road
Springfield, VA 22161

NTIS price codes
Printed copy: A05
Microfiche copy: A01

Distribution
Category UC-35

SAND85-0708
Unlimited Distribution
Printed April 1985

SCAP - A Shaped Charge Analysis Program - User's Manual for SCAP 1.0

A. C. Robinson
Computational Physics & Mechanics Division II
Sandia National Laboratories
Albuquerque, New Mexico 87185

ABSTRACT

The basic modeling and format for a shaped charge analysis program, SCAP, is described. The code models the motion of liner elements due to explosive loading, jet formation, jet breakup and target penetration through application of a series of analytical approximations. The structure of the code is intended to provide flexibility in shaped charge device and target configurations and in modeling techniques. The code is designed for interactive use and produces both printed and plotted output. Examples of code output are given and compared with experimental data.

Acknowledgment

I wish to thank M. G. Vigil for numerous discussions and much encouragement during the development of SCAP. His enthusiasm and interest have been much appreciated.

Contents

	Page
Acknowledgment	2
1 Introduction	5
2 Background	7
3 Initialization and Discretization	9
4 Liner motion	12
5 Jet Formation	20
6 Jet Breakup	24
7 Penetration	26
8 Experimental Comparison and Discussion	29
References	38
Appendix A - Incremental Area between Two Curves	40
Appendix B - Integrals of Acceleration Functions	41
Appendix C - Code Structure, Subroutines and Variables	43
Appendix D - Input and Output	51
Appendix E - Sample Run Sequence	57

Figures

	Page
Figure 1. SCAP coordinate system and zoning options.	10
Figure 2. Comparison of acceleration modeling with Gurney formula. Gurney model (line); impulsive (circle); constant (cross); ex- ponential (triangle); modified exponential (x).	14
Figure 3. Liner motion; physical plane. Original liner position (dotted), current liner position (solid), detonation front (dashed).	16
Figure 4. Liner motion; (ξ -t) plane	17
Figure 5. Jet formation diagram	21
Figure 6. Velocities as a function of original axial position for Allison and Vitali charge.	31
Figure 7. Penetration versus original axial location and time from initiation for Allison and Vitali charge.	32
Figure 8. Penetration versus standoff for 20° copper liner and steel target.	33
Figure 9. Penetration versus standoff for 40° copper liner and steel target.	34
Figure 10. Penetration versus standoff for 60° copper liner and steel target.	35
Figure 11. Penetration versus standoff for 90° copper liner and steel target.	36
Figure 12. Velocities as a function of original axis position for 20° copper liner.	37
Figure 13. Incremental Area Vectors	40

1 Introduction

SCAP (Shaped Charge Analysis Program) is an interactive modeling code developed at Sandia National Laboratories for the purpose of assisting in the design of shaped charge components. Design requirements for Sandia applications need not correspond to typical conventional weapon shaped charge requirements. Miniaturized components, specialized materials and non-standard designs open the way for possible unique modeling requirements. The need for an in-house Sandia code with maximum modeling flexibility and ease of use has lead to the development of SCAP.

SCAP is user friendly and very inexpensive to run. It is designed for flexibility in shaped charge device configuration, choice of competing modeling techniques, and implementation of new models for various parts of shaped charge jet formation and penetration phenomena. The code at present contains models for liner acceleration, jet formation, jet stretching and breakup, jet penetration and confinement motion. Different models are available for some portions of the code and may be chosen via a menu format. Few *a priori* assumptions are built into the code with the intent that the program structure should allow the modeling of devices of nonstandard design. For example, derivatives needed in the analysis are computed via interpolation rather than from formulas based on geometric assumptions. The result is a code which is conceptually simple and well structured.

SCAP is written in FORTRAN 77 and is currently run on VAX systems at Sandia. The code produces both hardcopy output listings and plotted output. Plotting portions of the code allow creation of a movie of the jet formation process and utilize the high-level plotting package, DISSPLA, a proprietary product of Integrated Software Systems Corporation of San Diego, California. DISSPLA is coupled to the Sandia Virtual Device Interface (SVDI) system which allows use of the same code on any supported plotting device. Thus, any Sandia supported black and white or color plotting device may be used with SCAP. The code is most convenient to run on dual alphanumeric and graphics terminals. The code also accesses an ordinary differential equation solver in the Sandia SLATEC mathematical subroutine library. Sandia personnel may obtain information and/or assistance relative to DISSPLA, SVDI and the SLATEC library from the Computer Consulting and Training Division (2614). However, the SCAP user need not be familiar with the details of these systems. The user must only obtain the appropriate SVDI device codes for his particular plotting output devices.

Section 2 gives background information on shaped charge phenomena and gives the rationale behind the use of a shaped charge analysis code. Initialization and zoning formats for the code are discussed in Section 3. Section 4 discusses liner acceleration and motion. The jet formation, jet breakup and jet penetration models are described in Sections 5, 6 and 7, respectively. Section 8 provides a short comparison of code results with experimental data. A more extensive comparison with experimental data is planned for release in a future Sandia report. Appendix A derives formulas for computing incremental areas or volumes used in the modeling. Appendix B gives formulas used in the liner position and velocity subroutine. Appendix C documents code structure, subroutines and variables used in the code. Appendix D describes the required data input stream for the current version of the code. Appendix E gives a SCAP run sequence with the resulting plotted and printed output for one of the sample cases discussed in Section 8.

As mentioned above, SCAP is designed for ease of model modification and/or addition through its sequential modular design and the interactive capability for choosing competing models. At this time the code appears to be a useful tool for shaped charge design. This user's manual documents the first version, SCAP 1.0. Future interaction with the component design user community at Sandia will lead to additions, improvements and modifications to the code. As circumstances warrant, further revisions of the code and/or user's manual will be released.

2 Background

The term "shaped charge" refers to the use of a high-explosive charge to accelerate a metal cone or wedge in such a way that a very high velocity metallic jet is produced at the collapse point. This jet typically stretches to several times its original length before it breaks up into small particles. The shaped charge jet is useful for many applications because of its good penetration capability. Armor piercing conventional weapons applications have, traditionally, provided much of the impetus for the study and development of shaped charges. Much modeling and development occurred during World War II. Shaped charges also find utility in many industrial applications including wellbore perforation, underwater trenching and demolition (DeFrank, 1972). Applications related to the mining industry and many early references are given by Austin (1959). Any situation where cutting or perforation in a precise and directed way is essential may be appropriate for shaped charge application.

Typically two approaches have been taken to the problem of modeling the shaped charge. The first approach involves the use of so-called "hydrocodes" to compute directly the flow pattern and principal characteristics of the shaped charge (e.g., Sedgwick, et. al., 1972). These codes typically solve the full set of mass, momentum and energy balance equations of continuum mechanics using difference approximations to the governing differential equations. This approach has the advantage of being able to apply many of the known physical properties of different materials and explosives in the modeling scheme. Equation of state properties and material strength effects are taken into account. However, the disadvantage is that the computations are usually very expensive and require access to very fast computers with large amounts of memory. The computations involve very high strains and strain rates in the small jetting region. A single run may involve a great deal of time and effort on the part of the shaped charge designer. Extensive parametric studies are often not practical or economically acceptable.

A second approach abandons the idea of a direct finite difference or finite element approach to solving continuum equations of motion. Instead one pieces together analytical models which attempt to describe portions of the shaped charge jet phenomenon. The first attempt of this type appears to be the work of Pugh, Eichelberger and Rostoker (1952) who applied the basic jet theory of Birkhoff et. al. (1943) to the non-steady collapse phenomena. In fact, no major changes in conceptual approach have been devised since this work. The

major impetus has been toward a better understanding and modeling of various elements of the shaped charge phenomena. One must model detonation wave characteristics, acceleration of the metal liner, jet formation, stretching and particulation of the jet, and penetration to obtain complete information on the effect of the shaped charge jet. Several codes of this type have been written. For example, a code used by the Ballistic Research Laboratory, BASC, is described by Harrison (1981). His report includes numerous references. SCAP is similar to the BASC code in conceptual approach but is structured for additional flexibility in order to conveniently treat component design problems that arise at Sandia.

In an analytical shaped charge code, the modeling of the shaped charge phenomena need not be so intimately connected in space and time as in a finite difference hydrocode. The results from the application of one model may be saved for use by the models for "subsequent" phenomena irrespective of the actual times in which the events occur for individual elements. For example, the acceleration and velocity characteristics for all portions of the liner may be computed before the jet formation portion of the code is entered. The code may compute a representation of the location of each element of the jet as a function of time, before any penetration computations are attempted, even though the standoff may be so short that penetration and jet formation in reality occur simultaneously for different liner elements. Codes utilizing analytical models can thus provide a tool for quickly and easily assessing the performance of a given shaped charge configuration. A typical calculation time would be a few seconds on a medium size computer such as a VAX11/780 and a few minutes on a small personal computer.

The disadvantage of an analytical shaped charge code is that, of necessity, one simplifies much of the physics of the problem. The equations of state of the various materials (explosive, liner, tamping or confinement, and target) are not utilized, and therefore detailed shock propagation variables, wave interactions, pressures, densities and related shock physics are not included in an analytical code. However, the most important characteristics of the shaped charge phenomena can be modeled with sufficient accuracy to provide useful information for preliminary engineering design. Typically, such a code is used in conjunction with an experimental, and perhaps a more intensive computational, program and is clearly useful for parametric studies. An analysis code is designed to reduce experimental and computational effort on the part of the shaped charge designer.

3 Initialization and Discretization

In a conical shaped charge the explosive is detonated at one end of the charge, and the detonation wave collapses the liner as it sweeps past. SCAP assumes a constant detonation velocity. Thus geometrical considerations give arrival times at specific points in the shaped charge. Acceleration of the liner and confinement after the arrival of the detonation front is computed from the Gurney method for finding the velocity of explosively driven plates or cylinders. This method is described in Section 4. Since the shaped charge does not have the simple geometry of one of the Gurney formulas, the formulas are applied to small zones along the length of the charge. In this way differences in the thickness of the liner, confinement and explosive show up in the estimated liner velocity for each region of the charge. A linear shaped charge is modeled by an instantaneous detonation throughout the charge cross-section.

The liner acceleration modeling in SCAP divides the liner, explosive and confinement into NZ incremental units or zones. Unless specifically changed by the user, NZ is chosen by the code to give a zone size approximately on the order of the liner thickness. A basic assumption inherent in the code is that the motion of the liner and confinement can be determined from the expected acceleration of the individual elements using a model which takes into account the mass of the liner, explosive and confinement corresponding to each zone.

Figure 1 illustrates the basic SCAP coordinate system and the two basic options available for the explosive zoning. The free side and explosive sides of the liner are defined by the entry points RLIN1 and RLIN2, respectively, in the subroutine RLIN. The routines return $(x(\xi), y(\xi))$ position values of the surfaces as a function of a parameter ξ which varies from zero to one. The value $\xi = 0$ corresponds to the liner apex and $\xi = 1$ corresponds to the position at the liner base. The variable x is the axial location and y is the radial location. By definition, the top of the liner on the explosive side is at $x = 0$. The entry points RCON1 and RCON2 in the subroutine RCON give the interior and exterior surfaces of the confinement or tamper as a function of x (not ξ). The current coding allows modeling of linear liner and confinement surface shapes. The slopes of the inner and outer surfaces of the liner or confinement need not be the same which allows for tapered thicknesses. A single slope is allowed for each of the two surfaces of the liner. The confinement definition routine allows for a single slope discontinuity for each of the inner and outer tamper surfaces. Curved surfaces

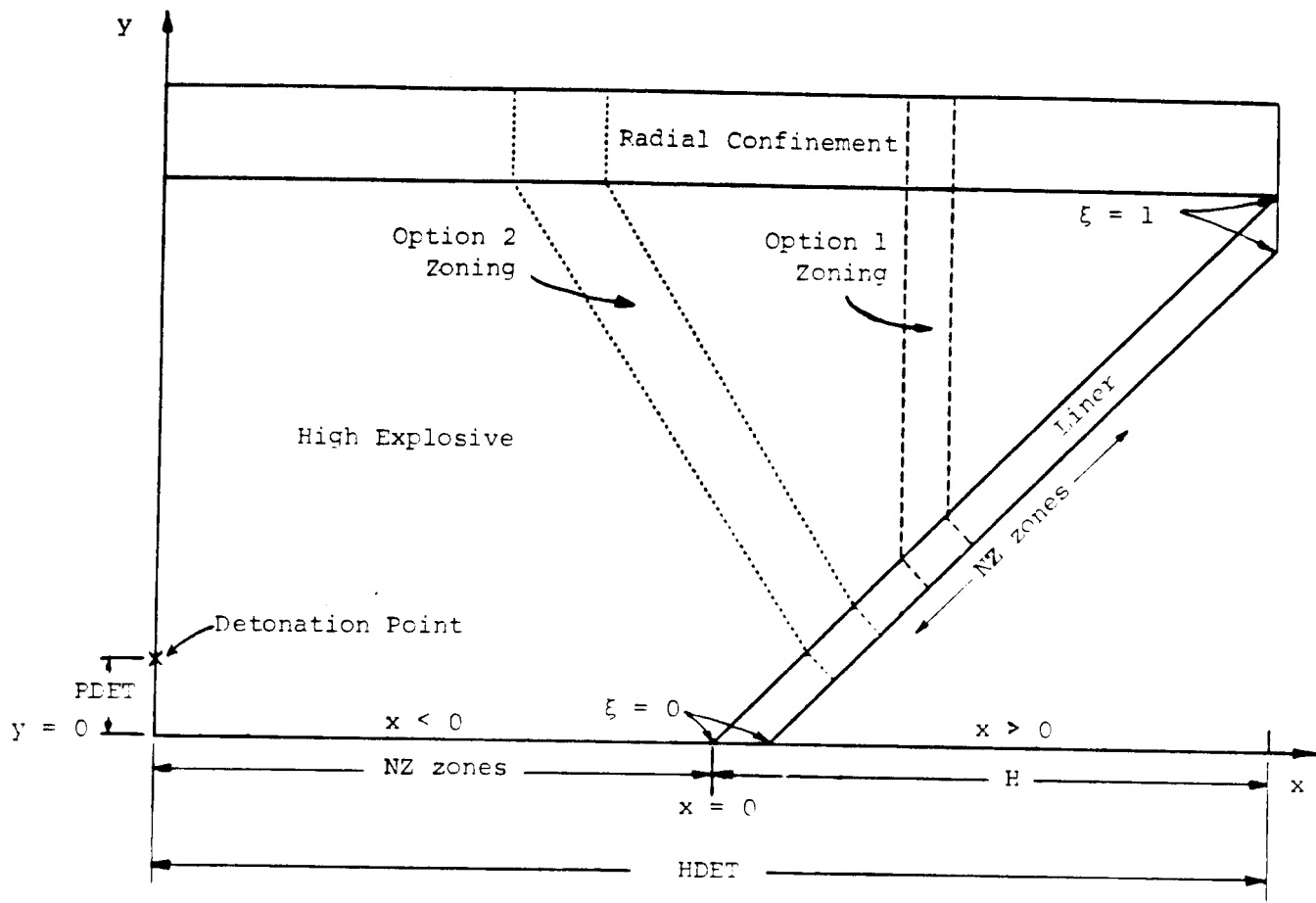


Figure 1. SCAP coordinate system and zoning options.

could also be implemented in RCON and RLIN but are not current options in the code.

As shown in Figure 1, SCAP assumes symmetry about the charge axis for both linear and conical shaped charges. In practice, this symmetry may be difficult to achieve but is important for reproducible charge performance. The first option assumes that the explosive used to accelerate the confinement and liner is found in a radial direction from the liner element. This is the default option used in the code. The second option uses the amount of explosive along the line connecting the point of the detonation front on the confinement to the detonation front at ξ . The number, NZ, indicates the number of zones used for liner and confinement acceleration modeling. An equal number of zones is used for $x < 0$ to compute the confinement velocity. The formulas used to compute the volumes of the liner, explosive and confinement elements are given in Appendix A. The volumes are needed to determine total incremental mass of liner, explosive and confinement for use in the Gurney analysis described in Section 4.

SCAP is intended to model linear and conical shaped charges where the basic mechanism of jet formation is the collapse of liner elements due to explosive loading followed by hydrodynamic jetting. Other types of lined cavity charges such as hemispherical charges and self-forged fragment charges, where the important liner projection mechanisms are not simply hydrodynamic jetting, or where the explosive zoning should be different than that used in current options, would require modeling in addition to that currently available in the code. Clearly, the current zoning options would not be appropriate for hemispherical liners near the charge axis. The parameterization of the liner by ξ rather than x in SCAP provides an appropriate structure for modeling these other types of lined-cavity charges. For example, the derivative of the liner surface, y , with respect to x at the axis for a hemispherical liner is unbounded, while a ξ parameterization can be chosen so that the derivative of $(x(\xi), y(\xi))$ with respect to ξ is well-defined.

4 Liner motion

Any shaped charge liner has a finite thickness, but in SCAP the liner is parameterized by a single variable, ξ , along its length. The position of the liner at any time can then be represented conveniently by a complex vector, $z(\xi, t) = x(\xi, t) + iy(\xi, t)$, denoting the position of the Lagrangian point ξ of the liner at time t . The velocity and acceleration of point ξ are given by the first and second partial derivatives of z with respect to t . In the code, $z(\xi, 0)$ is defined as the simple vector average of the points defined in the routine RLIN at the inner and outer surface of the liner at ξ . The assumed vector equation of motion for the liner, which expresses the assumptions that the history profile of the magnitude of the acceleration of the material elements is known and that the direction of the acceleration is normal to the current position of the liner, is given by the nonlinear partial differential equation

$$\frac{\partial^2 z}{\partial t^2} = -i \frac{V(\xi)}{\tau(\xi)} f\left(\frac{t - T(\xi)}{\tau(\xi)}\right) \frac{\partial z / \partial \xi}{|\partial z / \partial \xi|}, \quad t > T(\xi) \quad (4.1)$$

$$\frac{\partial^2 z}{\partial t^2} = 0, \quad t \leq T(\xi) \quad (4.2)$$

The quantity $T(\xi)$ is the time at which the detonation front arrives at point ξ and can be determined from geometrical considerations and the known denotation velocity of the explosive. The nonnegative real function $f(\eta)$ is termed the acceleration function and has unit area on the interval $0 \leq \eta < \infty$. The function $V(\xi)$ is the final speed the liner would achieve for configurations which do not change the liner normal during the acceleration period, and $\tau(\xi)$ is a measure of the acceleration time for the liner element. The right hand side of equation (4.1) is the force per unit mass acting on a liner element. We emphasize that the choice of complex notation is purely a matter of notational convenience, ease of algebraic manipulation and programming convenience. Equation (4.1) is equivalent to a coupled pair of real equations.

The functions V , τ and f in equation (4.1) can be chosen to match experimental data or two-dimensional hydrocode studies (Chou, et. al., 1981; Chou, et. al., 1983). Alternatively, they may be chosen to fit an acceleration model such as the Gurney method (Bertholf, 1983; Jones, et. al., 1980; Kennedy, 1970); this is the current method for determining these values in the code. The derivation of the Gurney formulas used in the code is given by Jones, et. al. (1980).

The Gurney formula for an asymmetric sandwich configuration gives the flyer velocity, V_G , as a function of flyer position, d , as

$$V_G^2 = \frac{2E}{B} \left(1 - \left(\frac{d}{d_0}(A+1) - A \right)^{-B/F} \right) \quad (4.3)$$

where d_0 is the initial thickness of the explosive, E is the specific Gurney energy and

$$A = (1 + 2M/C)/(1 + 2N/C), \quad F = (M/C)(A+1)/(\gamma-1)$$

$$B = \frac{1+A^3}{3(1+A)} + \frac{N}{C}A^2 + \frac{M}{C},$$

where M is total flyer mass, N is the total tamper mass, C is the total explosive mass and γ is the adiabatic coefficient of expansion for the explosive. Differentiation with respect to time gives the following results at $d = d_0$ (or $t=T$):

$$\frac{dV_G}{dt}(d_0) = \frac{E(A+1)}{Fd_0}, \quad \frac{d^2V_G}{dt^2}(d_0) = 0. \quad (4.4)$$

Our assumed form for the acceleration (4.1) allows for an arbitrary unit area function f and free parameters τ and V . The code sets τ and V in (4.1) by matching the velocity at $d = \infty$ and the acceleration at $d = d_0$ with the corresponding values from the Gurney formula (2.4). Thus we obtain

$$V = \sqrt{2E/B}, \quad \tau = VFd_0f(0)/(E(A+1)). \quad (4.5)$$

We still have considerable flexibility in the f function for the shape of the acceleration profile, and many refinements are certainly possible. For example, since the second time derivative of V_G at $d = d_0$ is identically zero we may choose an acceleration function f with this property. In the code the user has a choice of several functions f , described in Appendix B. Figure 2 compares a typical velocity versus distance diagram using the several fits corresponding to the acceleration functions of Appendix B. The default fit used in the code is the modified exponential function. This function satisfies both of equations (4.4), and, as seen in Figure 2, gives the best fit to the Gurney acceleration profile. Other choices for f and other matching schemes for V and τ could be implemented.

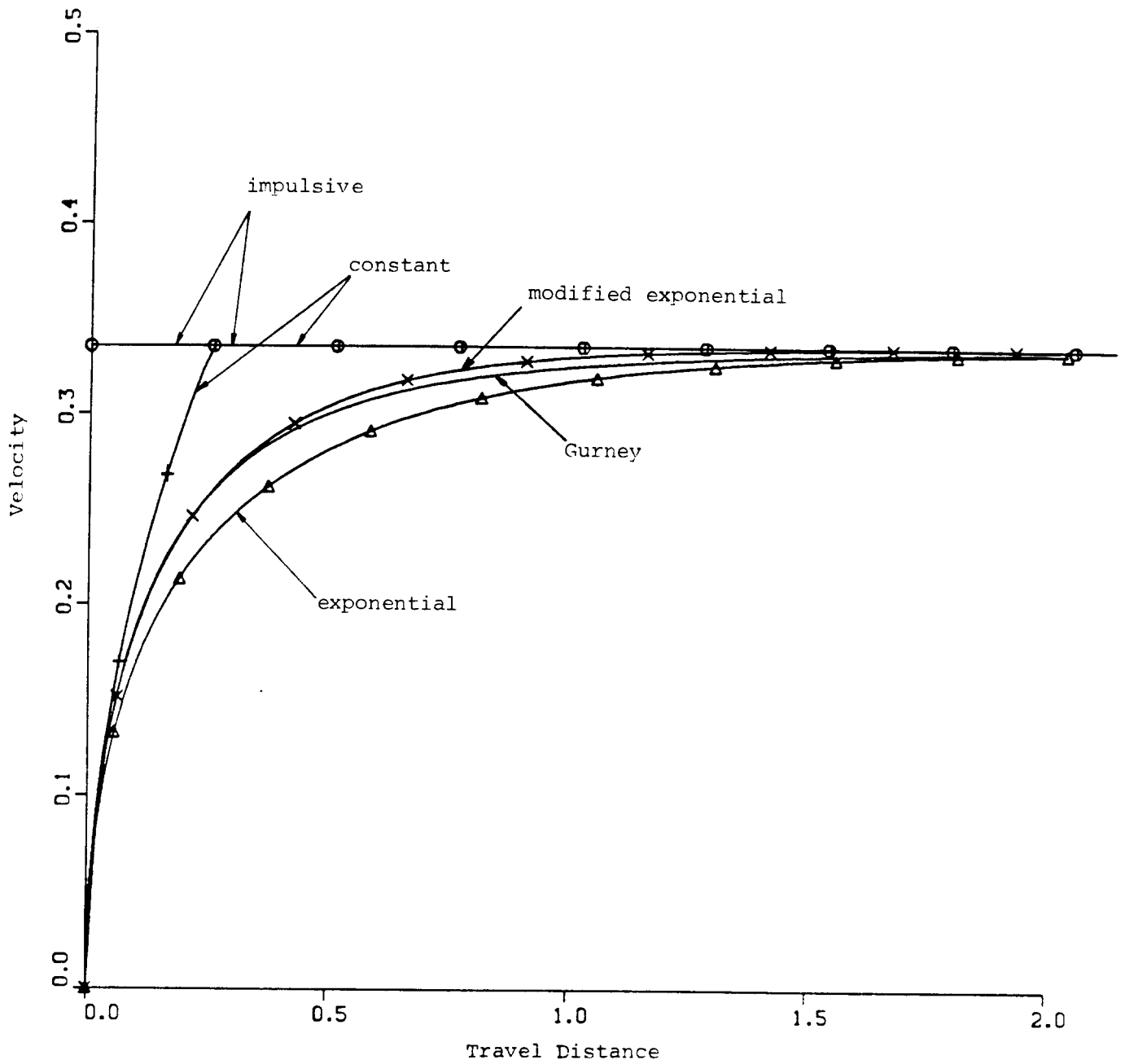


Figure 2. Comparison of acceleration modeling with Gurney formula.
 Gurney model (line); impulsive (circle); constant (cross);
 exponential (triangle); modified exponential (x).

The confinement motion for zones including the liner is modeled using an impulsive acceleration model with the confinement velocity determined by the formula (4.3) at $d = \infty$ with M and N switched. For the zones corresponding to $x < 0$ on the axis, the Gurney formula for the confinement velocity, V_c , is

$$V_c = \sqrt{2E} \left[\frac{N}{C} + \frac{1}{4 - IGEOM} \right]^{-1/2} \quad (4.6)$$

where $IGEOM = 1$ for a linear shaped charge and $IGEOM = 2$ for a conical shaped charge. Note that the Gurney modeling used in the code for the liner and confinement acceleration does not depend on $IGEOM$. The flat plate Gurney model is used to compute accelerations using the appropriate mass for the geometry (See Appendix A). The Gurney modeling for conical shaped charge liner acceleration may need to be improved perhaps along the lines suggested by Chou, et. al. (1983). For graphical purposes, we use the Taylor formula, $\sin(\delta) = V_c/2U$, where δ is the velocity deflection angle from the normal and U is the detonation velocity component parallel to the confinement, to compute the direction of motion of the confinement (Harrison, 1981).

We assume that the liner is motionless at the time of arrival of the denotation wave so that we have the initial conditions

$$z(\xi, T) = z_0(\xi); \quad \frac{\partial z}{\partial t}(\xi, T) = 0. \quad (4.7)$$

Figures 3 and 4 show the configuration of the liner in both physical and (ξ, t) space.

Equation (4.1) is nonlinear and difficult to solve in any generality. However, the equation is amenable to application of perturbation theory. The results of an asymptotic analysis give formulas for the motion of the liner (Robinson, 1984). For $t > T$ the position and velocity of each element of the liner are given by

$$z(\xi, t) = z_0 - i\tau V e^{i\theta_0} \left[f_1 - \frac{i}{|z'_0|} \{ (\tau V)' f_2 - V \tau' f_3 - VT' f_4 \} \right] \quad (4.8)$$

and

$$\frac{\partial z}{\partial t}(\xi, t) = -iV e^{i\theta_0} \left[\frac{df_1}{d\eta} - \frac{i}{|z'_0|} \left\{ (\tau V)' \frac{df_2}{d\eta} - V \tau' \frac{df_3}{d\eta} - VT' \frac{df_4}{d\eta} \right\} \right] \quad (4.9)$$

where $\eta = (t - T)/\tau$, the prime represents differentiation with respect to ξ and

$$f_1(\eta) = \int_0^\eta (\eta - s) f ds, \quad f_2(\eta) = \int_0^\eta (\eta - s) f f_1 ds$$

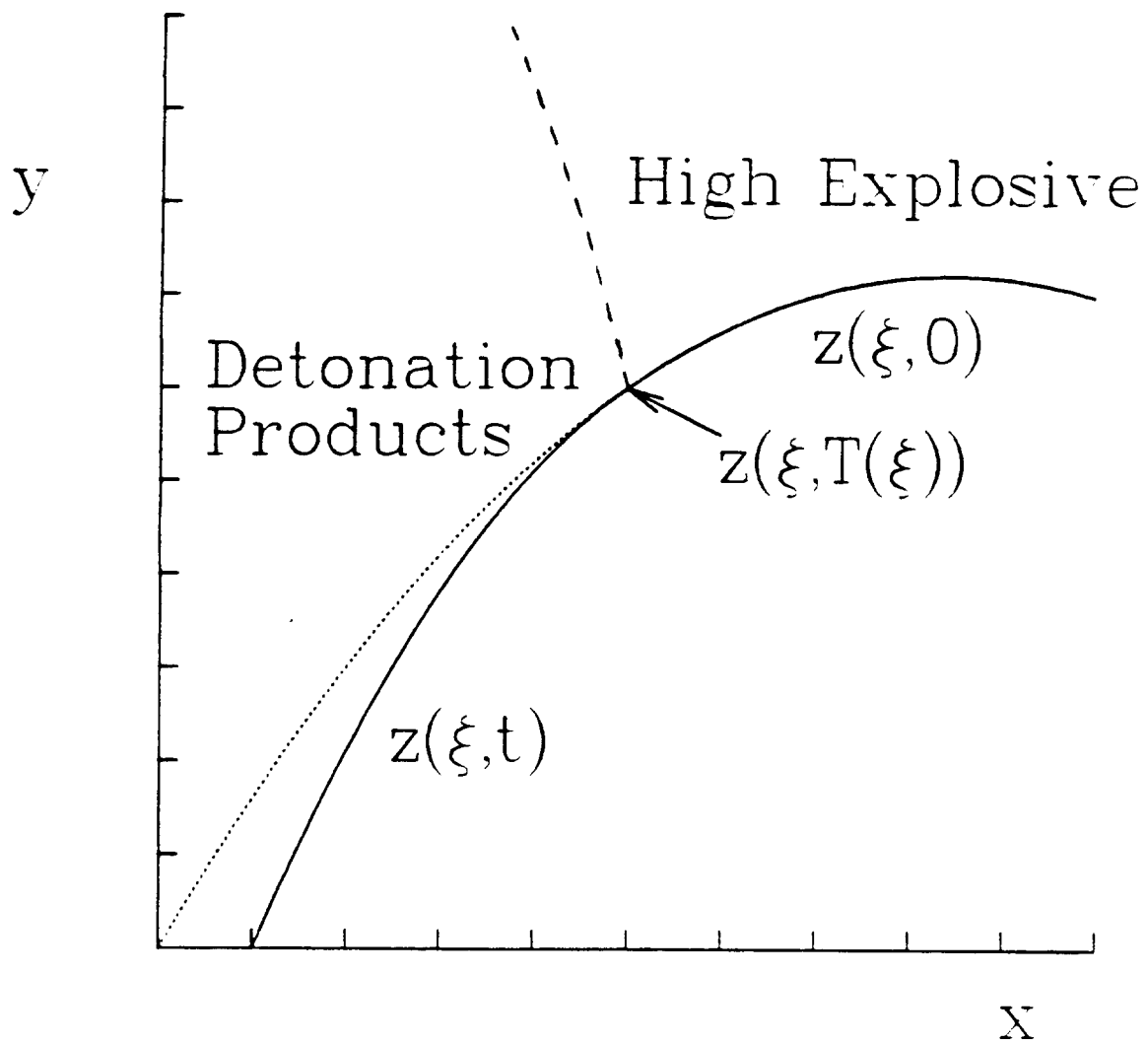


Figure 3. Liner motion; physical plane. Original liner position (dotted), current liner position (solid), detonation front (dashed).

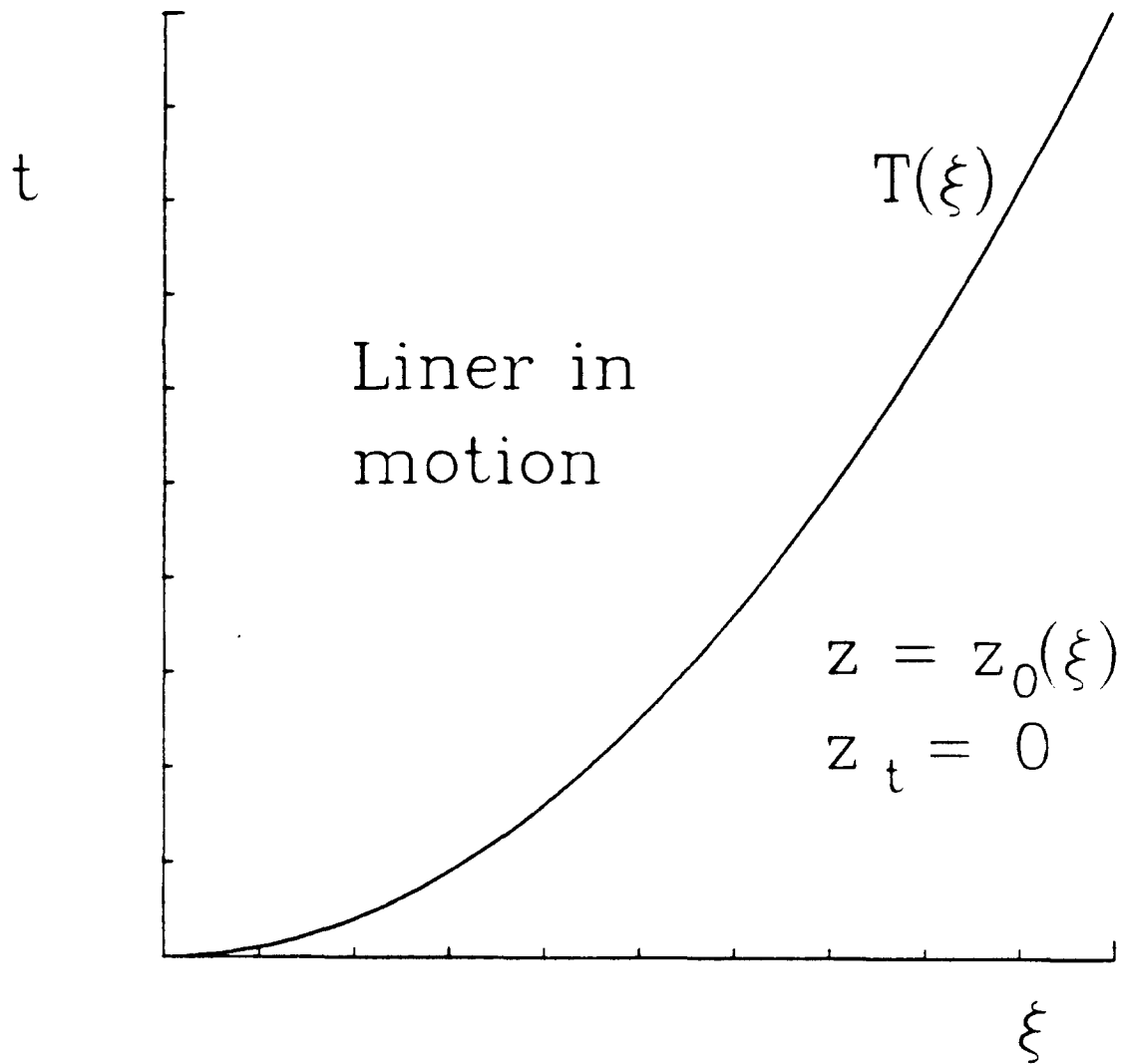


Figure 4. Liner motion; $(\xi-t)$ plane

$$f_3(\eta) = \int_0^\eta (\eta - s) s f \frac{df_1}{ds} ds, \quad f_4(\eta) = \int_0^\eta (\eta - s) f \frac{df_1}{ds} ds.$$

Appendix B gives values of the f integrals for four possible choices of the acceleration function.

Although the curvature (if any) of the liner does not enter explicitly into the formulas for the position and velocity of elements of the liner, it does enter implicitly through $T(\xi)$ and may also through $|z'_0|$. One expects the error in equations (4.8-4.9) to be $O(\epsilon^2)$ uniformly for η in $[0, 1/\epsilon]$ as ϵ tends to zero with $\epsilon = O(\mathcal{V}/\mathcal{U})$ where \mathcal{V} is a measure of the final liner velocity and \mathcal{U} is the detonation velocity. The order estimate assumes that the detonation wave travels the length of the liner in a typical acceleration time. In other words, the change, δ , in the projection direction from the original normal to the liner should be small.

A standard assumption made in analytical shaped charge codes is that the Taylor angle is achieved instantaneously so that the position of each element of the liner at any instant is

$$z(\xi, t) = z_0(\xi) - iV(t - T)e^{i(\theta_0 + \delta)} \quad (4.10)$$

where the angle δ is chosen from the Taylor formula, $\sin(\delta) = V/(2U)$, and U is the component of the detonation velocity parallel to the liner. This equation is included as a special case of (4.8-4.9) by taking the limit $\tau \rightarrow 0$ with $t > T$ or, equivalently, setting $f(\eta)$ equal to the one-sided Dirac delta function. From equation (4.8) and Appendix B1 we have in this case

$$z = z_0 - iV(t - T)e^{i\theta_0} \left\{ 1 + \frac{i}{|z'_0|} \frac{VT'}{2} \right\}. \quad (4.11)$$

The equations (4.10) and (4.11) clearly correspond through linear terms in δ for small δ since $T'/|z'_0| = 1/U$.

Equations (4.8-4.9) have the advantage of including directly the effect of finite acceleration in the position and velocity of the liner. In SCAP we obtain a rational estimate for the position and velocity of a liner element ξ no matter how small $t - T(\xi)$ is. Thus, the appearance of the so-called *inverse velocity gradient* (Harrison, 1981) in jet formation modeling occurs automatically by direct application of the formulas with a finite acceleration time.

Although equations (4.8-4.9) have the disadvantage that we cannot solve directly for the arrival time of a liner element at a given y value, as is the standard technique using equation (4.10), this provides no great difficulty. The

subroutine ZXT calculates the position and velocity of a liner element at any given time using equations (4.8-4.9). It is a straightforward matter to compute the time at which the element arrives at a specified y value, y_{clps} , which is near the axis of the shaped charge, by application of a Newton iteration scheme. This time is the collapse time at the axis when the element is at the collapse point. The position, velocity, local liner angle and any other desired quantity can then be computed from the formulas (4.8-4.9). These values are used to compute the jet and slug velocities for each element from the Pugh, Eichelberger and Rostoker (1952) theory as described in Section 5. The procedure works very well as long as some care is taken to iterate to the proper root in $t > T$ rather than the root in the continuation of the solution in $t < T$.

The choice of the collapse point, y_{clps} , essentially selects the time, and thus the velocity, at collapse. However, it is not immediately obvious what this value should be. One possibility is $y_{clps} = 0$. This is option IAXIS = 1 in the code. Another possibility is to take into account the finite volume of the element, and since the point, z , is at the approximate center of the element, a position for this center at the collapse time can be estimated from the known volume of the element. For cylindrical geometry one might specify that for a given element volume, dv ,

$$\pi(2y_{clps})^3 = dv \Leftrightarrow y_{clps} = (dv)^{1/3}/2.93 \quad (4.12)$$

or

$$2\pi^2 y_{clps}^3 = dv \Leftrightarrow y_{clps} = (dv)^{1/3}/2.70 \quad (4.13)$$

for cylindrical and toroidal shaped volumes at collapse, respectively. For plane geometry we have

$$2(2y_{clps})^2 = dv \Leftrightarrow y_{clps} = (dv)^{1/2}/2.83 \quad (4.14)$$

We then choose

$$y_{clps} = (dv)^{\frac{1}{1+IGEOM}}/2.8 \quad (4.15)$$

as a reasonable estimate for a collapse radius. A larger radius would have the effect of emphasizing the inverse velocity gradient, while a smaller radius would tend to remove this effect. This ad hoc model, IAXIS = 2, is the current default option.

5 Jet Formation

We apply the basic theory of Pugh, Eichelberger and Rostoker (1952) for the computation of the jet and slug characteristics. Upon applying the iterative technique described in Section 4 to obtain the arrival time of the liner element, ξ , at the liner axis, we can then proceed to calculate the jet and slug velocities. A basic assumption invoked in the subsequent theory is that the collapse process is approximately a steady state in the frame of reference of the collapse point.

From the geometrical considerations of Figure 4, we can obtain the velocity of the stagnation point, V_{sp} , and the velocity of the flow coming into the stagnation point, V_f . The equations for these quantities are

$$V_f = V_0 \sin(\psi) / \sin(\beta) \quad (5.1)$$

$$V_{sp} = V_0 \sin(\pi - \beta - \psi) / \sin(\beta) \quad (5.2)$$

where $V_0 = |\frac{\partial z}{\partial t}|$ is the magnitude of the velocity of the incoming liner element, $\psi = -\arg \frac{\partial z}{\partial t}$ is the angle the velocity vector makes with the axis and $\beta = \arg \frac{\partial z}{\partial \xi}$ is the angle the liner makes with the axis. The theory assumes that the free streamline jet theory of an incompressible perfect fluid may be applied. Then, the velocity magnitude of the jet and slug in the frame of reference of the stagnation point is also V_f since the velocity is constant along the free streamlines. In the laboratory frame we have

$$V_j = V_{sp} + V_f, \quad V_s = V_{sp} - V_f \quad (5.3)$$

where V_j is the jet velocity and V_s is the slug velocity. The portion of the mass of the liner element going into the jet, dm_j , and slug, dm_s , is given from mass and momentum conservation by

$$dm_j = \sin^2(\beta/2) dm_l, \quad dm_s = \cos^2(\beta/2) dm_l \quad (5.4)$$

where dm_l is the mass of an element of the liner.

In practice, coherent shaped charge jets are not always seen. A relatively simple criterion has been discussed by Chou, et. al. (1976) for deciding whether a coherent jet will be formed. The criterion is based on the bulk sound speed, c , of the material of the liner. If $V_f/c < \kappa$ a coherent jet is formed, and we use

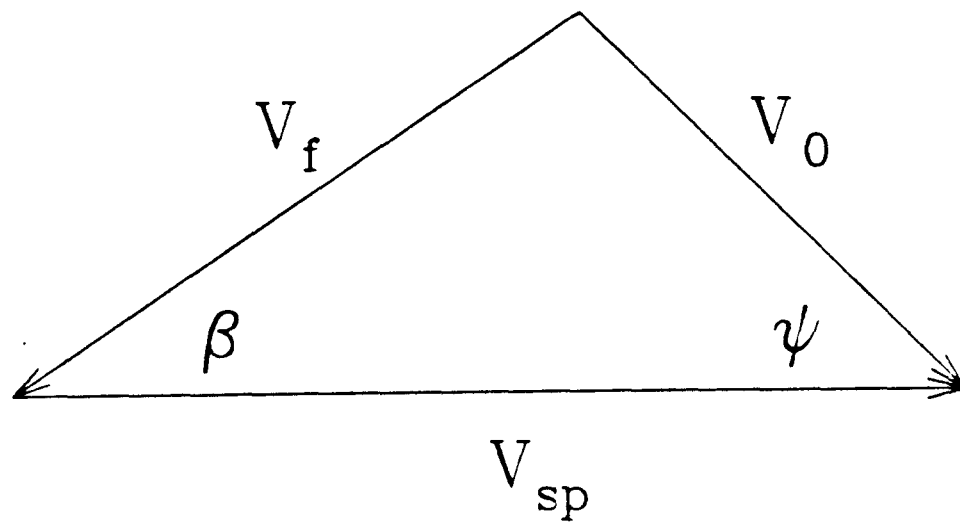


Figure 5. Jet formation diagram

the incompressible approximation (5.3-5.4). Chou, et. al. (1976) propose $\kappa = 1$, although, for copper, $\kappa = 1.23$ has been proposed based on experimental data (Harrison, 1981). If $V_f/c > \kappa$ a coherent jet is not formed, and it is assumed that a shock forms at the axis and no jetting occurs. In this case the code specifies

$$V_j = V_{sp}, \quad V_s = V_{sp} - V_f \cos(\beta) \quad (5.5)$$

$$dm_j = 0; \quad dm_s = dm_l \quad (5.6)$$

A no-jet condition will usually be observed in the jet velocity output by a sudden and abrupt drop in the jet velocity followed by an equally abrupt return to a higher velocity. The jet is assumed to be composed only of those elements which follow the last element with a no-jet condition. The no-jet condition will typically be achieved only for very small liner apex angles.

Once the jet and slug velocities have been computed, it is then desirable to predict where the element, ξ , which collapsed at time, $t_a(\xi)$, at position, $x_a(\xi)$, will be at time t . Unfortunately the velocity of the jet elements coming from near the tip of the liner may be slower than elements coming in from subsequent elements due to the fact that less time is available to accelerate the liner elements. This creates the so-called *inverse velocity gradient* mentioned in the previous section. The result is that faster moving elements eventually overtake the slower moving elements, and it is clear that some sort of interaction must occur. To overcome this difficulty, the code uses an inelastic collision model to revise the velocity profile so that the jet velocity is monotonically decreasing with respect to ξ and the slug velocity is monotonically increasing with respect to ξ . For each sequence of velocities with the wrong sign for the velocity gradient, we replace each of those velocities with the mass weighted average velocity. This process is repeated until no such velocity sequences remain. The position of the jet element is then computed from

$$x_j(\xi, t) = x_a(\xi) + (t - t_a(\xi))V_j(\xi) \quad (5.7)$$

$$x_s(\xi, t) = x_a(\xi) + (t - t_a(\xi))V_s(\xi) \quad (5.8)$$

The radius of the jet, r_j , is determined from the equation

$$\left(-\frac{\partial x_j}{\partial \xi} d\xi \right) (\pi r_j^2) = dm_j / \rho_j \quad (5.9)$$

for cylindrical geometry and

$$\left(-\frac{\partial x_j}{\partial \xi} d\xi \right) (2r_j) = dm_j / \rho_j \quad (5.10)$$

for linear geometry where ρ_j is the jet density. The jet density is assumed equal to the liner density. The minus sign arises from the sign reversal of the ξ parameterization after jetting when the jet elements corresponding to the smallest values of ξ are the elements with largest x_j . Similar equations are used for the slug radius. No minus sign occurs in the equations for the radius in this case.

6 Jet Breakup

A typical shaped charge jet stretches to several times its original length before breaking up into small particles. The jet breakup time is a critical parameter used in jet penetration modeling. This is because the particulated jet is no longer stretching, and penetration depth increases with effective jet length. SCAP jet breakup modeling includes three different options. Two options provide for jet breakup along the entire jet length at a single input time. The last option is a model still under development which determines a breakup time from a local criterion based on jet parameters and a dynamic yield stress for the jet.

The default option (IBREAK=1) requires the user to input a breakup time, t_b , for the jet as a time from detonation initiation, the basic time origin used for all computation in the code. This breakup time could be approximated from flash X-ray experimental data. The second option (IBREAK=2) requires the user to input a breakup time measured from the jet virtual origin. This is the breakup time often given in the literature and is given the symbol, t_1 . A virtual origin jet has a representation of the form

$$x_j(\xi, t) - x_0 = V_j(\xi)(t - t_0) \quad (6.1)$$

where $x_j(\xi, t)$ is the axial location of the Lagrangian element, ξ , and $V_j(\xi)$ is the velocity of the element. The virtual origin is the point (x_0, t_0) . If it is possible to determine individual jet particles in a sequence of flash X-ray pictures, one may plot the (x, t) positions of several particles and then extrapolate backward in time and space to determine an approximate virtual origin. The breakup time used in the code for this second option is $t_b = t_0 + t_1$. The virtual time origin, t_0 , is not input by the user but is computed internally from a least squares analysis of the jet velocity profile as predicted by SCAP modeling.

The code represents the jet in the form (5.7). If a virtual origin representation of the jet is assumed, then there exist x_0 and t_0 such that

$$x_0 = x_a(\xi) + (t_0 - t_a(\xi))V_j(\xi) \quad (6.2)$$

for every ξ . The output from the code will not be compatible with (6.2). However, (6.2) will often hold in an approximate sense. A standard linear least squares regression analysis with parameters x_0 and t_0 leads to an approximation for the virtual origin as well as a correlation coefficient giving the measure of fit.

This coefficient theoretically lies between -1 and 1 with a magnitude of 1 denoting a perfect fit. Jets from standard conical shaped charges appear to be well represented by a virtual origin approximation. The correlation coefficient from the code computation in these cases has typically been greater than .95. For the first two options, if t_b is less than the collapse time, $t_a(\xi)$, then t_b is set to $t_a(\xi)$ for each such ξ .

The third option (IBREAK=3) gives the breakup time of each element as a function of the radius and strain rate of the element at the collapse time, the jet density, and the dynamic yield stress of the jet material. This promising model is currently under development for the SCAP code. It is hoped that such a model will be available as the default model for future SCAP releases in order to enable more complete predictive capabilities.

7 Penetration

SCAP has the capability of modeling coherent and particulated jet penetration into one or more target layers. Penetration is computed by numerically solving an ordinary differential equation which represents the penetration process. The penetration model must be written in the form

$$\frac{dx_p}{dt} = g(x_p, t) \quad (7.1)$$

where $x_p(t)$ is the axial penetration position and g is obtained from a theory relating jet parameters to penetration velocity.

The only penetration model available in SCAP is a generalized version of the DiPersio, Simon and Merendino (1965) model developed at the Ballistic Research Laboratory. We term the BRL model and our model, DSM and GDSM, respectively. The GDSM theory invokes a quasi-steady state incompressible perfect fluid assumption to obtain the penetration velocity from Bernoulli's equation. Thus, in a frame of reference of the jet-target stagnation point we have

$$\rho_j \left(\frac{V_j - V_p}{\lambda} \right)^2 = \rho_t V_p^2 \quad (7.2)$$

where ρ_j , ρ_t , and V_p are the jet density, target density and penetration velocity, respectively. The quantity, λ , is equal to 1 for coherent jet penetration and accounts for a decrease in penetration rate after jet breakup. It must be a non-decreasing function of time. One can think of $1/\lambda$ as representing the probability that a penetration event is occurring at a given time. The product of this probability and the relative jet velocity represents an average relative velocity for the particulated jet. The probability is given by the ratio of the jet element length at breakup to the length of the jet at time t assuming no breakup. Thus

$$\lambda(\xi, t) = \max \left[1, \frac{\partial x_j(\xi, t)}{\partial \xi} / \frac{\partial x_j(\xi, t_b)}{\partial \xi} \right] \quad (7.3)$$

where $x_j(\xi, t)$ is the parametric representation of the jet. Solving for V_p in (7.2) and invoking the quasi-steady state assumption, we obtain

$$V_p = \frac{dx_p}{dt} = \frac{1}{1 + \mu\lambda(\xi, t)} V_j(\xi) \quad (7.4)$$

where $\mu = \sqrt{\rho_t/\rho_j}$ and ξ is that element of the jet which is at x_p at time t . From (5.7) we see that ξ is a root of

$$x_p = x_a(\xi) + (t - t_a(\xi))V_j(\xi) \quad (7.5)$$

for a given x_p and t . If no root exists then the penetration velocity is set to zero. Note also that if more than one target layer is present then μ depends on x_p . An option for several target layers is included for user convenience. However, the user should keep in mind that there may exist interface phenomena not modeled by the code which could result in serious difficulties in comparing SCAP modeling output and experimental data. For a limited number of interfaces the code should still be useful.

The DSM theory assumes a virtual origin approximation for the jet. That is, the jet may be represented in the form (6.1). Application of equation (7.3) yields the DSM result, $\lambda = \max[1, (t - t_0)/(t_b - t_0)]$. We should note that the DSM theory was not originally derived as described in the above paragraph but was obtained through a limiting process in which the number of jet particles was allowed to increase without bound. We now show that the GDSM theory reduces to the DSM theory for a more general representation of a virtual origin jet. Suppose there exists a virtual origin representation of (5.7). It follows that x_0 and t_0 exist such that (6.2) holds for every ξ . Also

$$\frac{\frac{\partial x_j}{\partial \xi}(\xi, t)}{\frac{\partial x_j}{\partial \xi}(\xi, t_b)} = \frac{x'_a + tV'_j - (t_a V'_j)'}{x'_a + t_b V'_j - (t_a V'_j)'} \quad (7.6)$$

Differentiating (6.2) with respect to ξ and substituting in (7.6), we see that the ratio (7.6) reduces to $(t - t_0)/(t_b - t_0)$ for a virtual origin jet. SCAP uses the formula (7.6) to compute λ . The GDSM theory has the advantage of being local in nature and not dependent on the validity of the virtual origin approximation. For example, if the charge configuration is such that there is no velocity gradient, we have $\lambda = 1$ irrespective of any assumed breakup time, and penetration will then be independent of standoff.

The equation (7.4) is solved using a general purpose ordinary differential equation solver, DERKF, found in the Sandia SLATEC subroutine library. This solver is capable of automatic startup, step size selection, and can detect and adjust for discontinuities in the derivative function g . The integration proceeds until $\frac{dx_p}{dt}$ reaches a minimum penetration velocity u_{min} input by the user. Note that u_{min} is *not* the minimum jet velocity. The value, u_{min} , is an empirically determined constant which accounts for the interaction of the jet and target material near the end of the penetration process when the assumption of

hydrodynamic flow is clearly not applicable and the effects of material strength become dominant. For typical applications u_{min} can be given a value of about $.15 \text{ cm}/\mu\text{sec}$.

8 Experimental Comparison and Discussion

In this section SCAP modeling output and experimental data are compared. The examples included here are intended to give the user a feel for SCAP modeling and output. We choose as a first example a case documented by Allison and Vitali (1962). The experiment consists of a lightly confined 105-mm diameter conical test charge with a copper liner and an apex opening angle of 42 degrees fired into a target of stacked steel plates. Figure 6 illustrates the code output for the different important modeling velocities described in the text. V is the velocity for the liner element determined by equation (4.5), V_0 is velocity of the liner at the collapse time, and V_j is the jet velocity of that portion of the liner element going into the jet. However, the two most important curves are the final or equilibrium jet velocity, which gives the value of V_j after application of the inelastic collision model, and the experimentally determined data points for the jet velocity. These two curves are indicated by arrows. The abscissa for Figure 6 is the original axial location of the jet elements normalized by the cone height.

Figure 7 shows three penetration curves. The curve which is concave down shows penetration depth versus time from detonation initiation. Thus SCAP modeling predicts a penetration rate which decreases with time. The other curves show predicted and experimental data of penetration depth versus the normalized initial axial position. It is interesting to note that most of the penetration is due to a small portion of the liner. This is a result of the effect of jet stretching on penetration. The modeling implemented a standard value for the Gurney velocity for Composition B and a u_{min} of .16 cm/ μ sec. Since no breakup time was available, the dynamic yield strength breakup time model was used since it had proved acceptable for the 40° liner mentioned below.

An excellent set of penetration standoff data for a series of shaped charges is found in DiPersio, Jones, Merendino and Simon (1967). We show in Figures 8, 9, 10 and 11 the penetration-standoff curves for a set of 1.5 inch diameter conical shaped charges with copper liners having apex angles of 20, 40, 60 and 90 degrees, respectively, fired into stacked .5 inch thick steel armor plates of hardness BHN 364-377. The Gurney velocity used was .3 cm/ μ sec which is about 10 percent greater than the nominal value for Composition B explosive. The Gurney velocity was increased since the jet tip velocity predicted was consistently low as compared to experimentally determined values. The reasons for the discrepancy for this set of experiments are unknown, but it should be noted that the Gurney velocity is typically accurate to about ten percent and is often much better

when calibrated for specific configurations (Kennedy, 1970, 1972). The manner in which the Gurney velocity, the zoning options and/or the y_{clps} value should be tuned for specific shaped charge geometries is a matter for further study. The jet virtual origin time was given in the experimental data. Therefore, the SCAP virtual origin breakup option was utilized for these computations. The minimum penetration velocity, u_{min} , was chosen using the optimal values for the DSM penetration theory determined by Shear, Brundick and Harrison (1981). The model prediction for all of the liners gives quite good agreement in the short standoff part of the penetration standoff curve. Errors are found to be on the order of ten percent. In the declining part of the penetration standoff curves, the agreement is good for the 40 and 60 degree liners but worse for the 20 and 90 degree liners although the general trend for the curves is acceptable. The error bars on the data curves are a one standard deviation value on each side of the mean curve. There were three tests at each standoff. It is interesting to note that the no-jet condition was achieved for part of the jet in the 10 degree liner case. The SCAP velocity output for this case is shown in Figure 12.

The above examples show that SCAP is capable of giving reasonable estimates of jet characteristics and penetration capabilities. It should also be apparent that two major handicaps exist for using SCAP to determine shaped charge performance. These are a knowledge of the shaped charge breakup time, t_b , and the minimum penetration velocity, u_{min} . However, even in cases where data are limited, SCAP may be used in conjunction with experiments to interpolate between designs and give indications of trends as design parameters are varied.

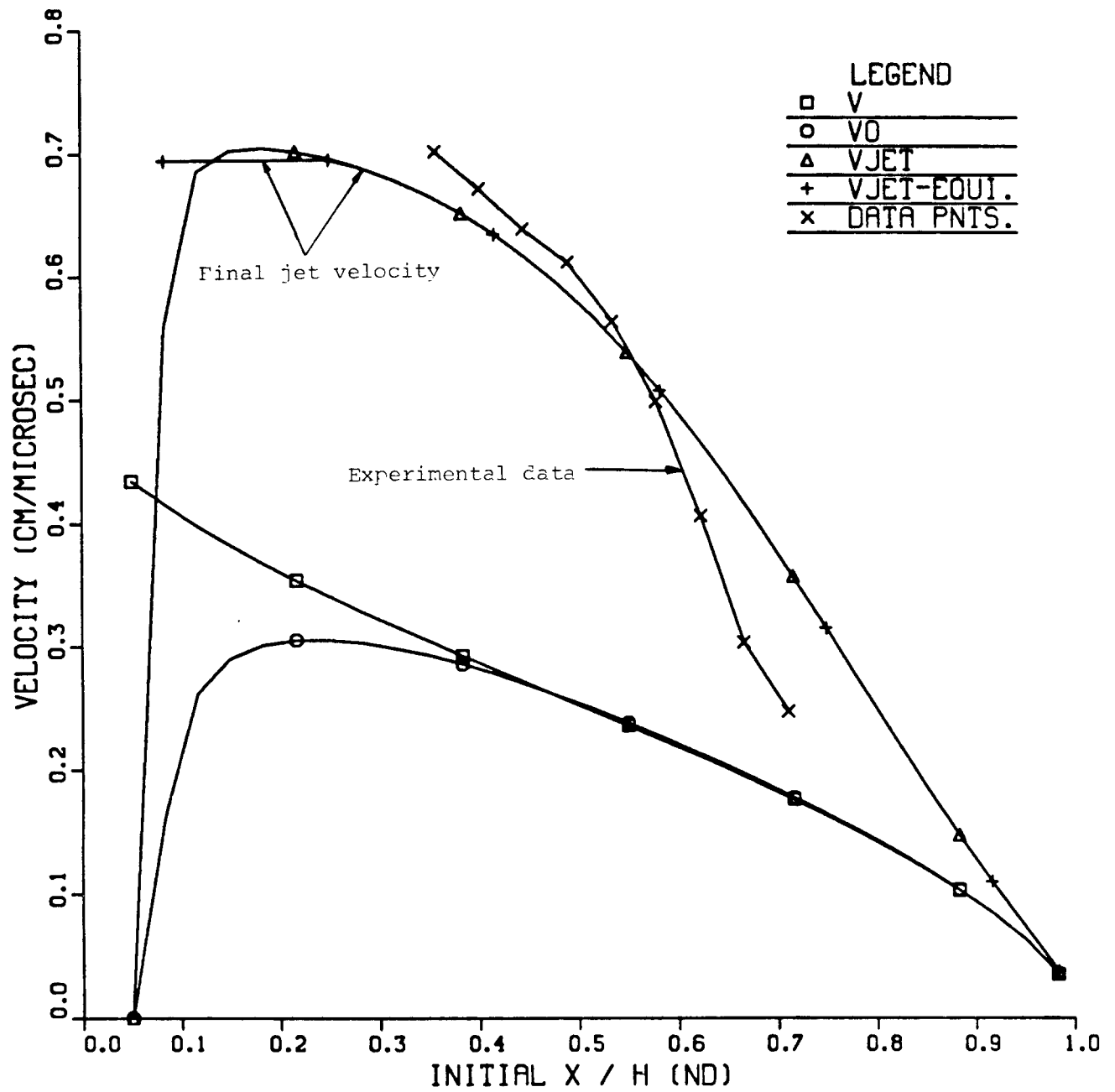


Figure 6. Velocities as a function of original axial position for Allison and Vitali charge.

PENETRATION AT 0.210E+02 (CM) STANDOFF

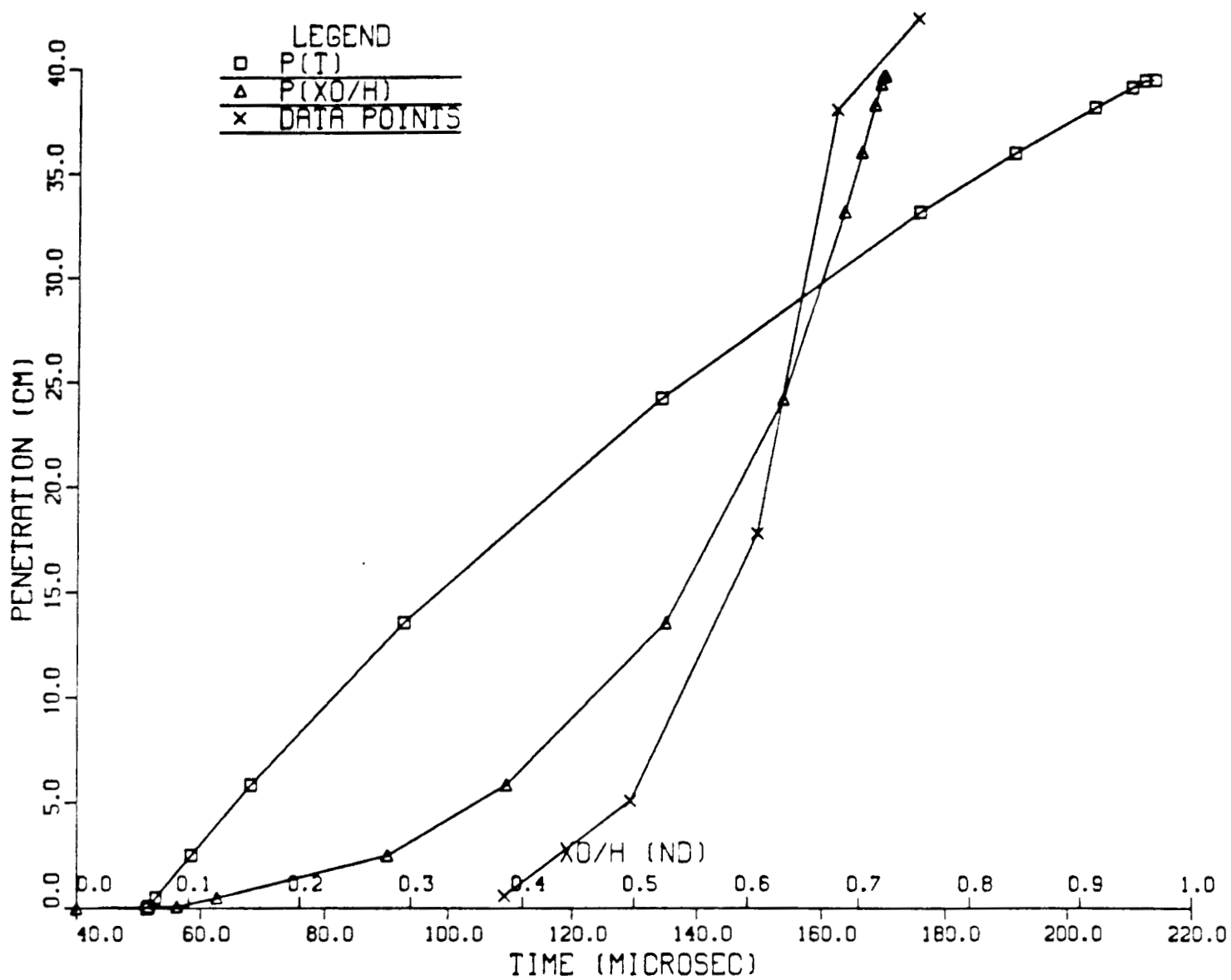


Figure 7. Penetration versus original axial location and time from initiation for Allison and Vitali charge.

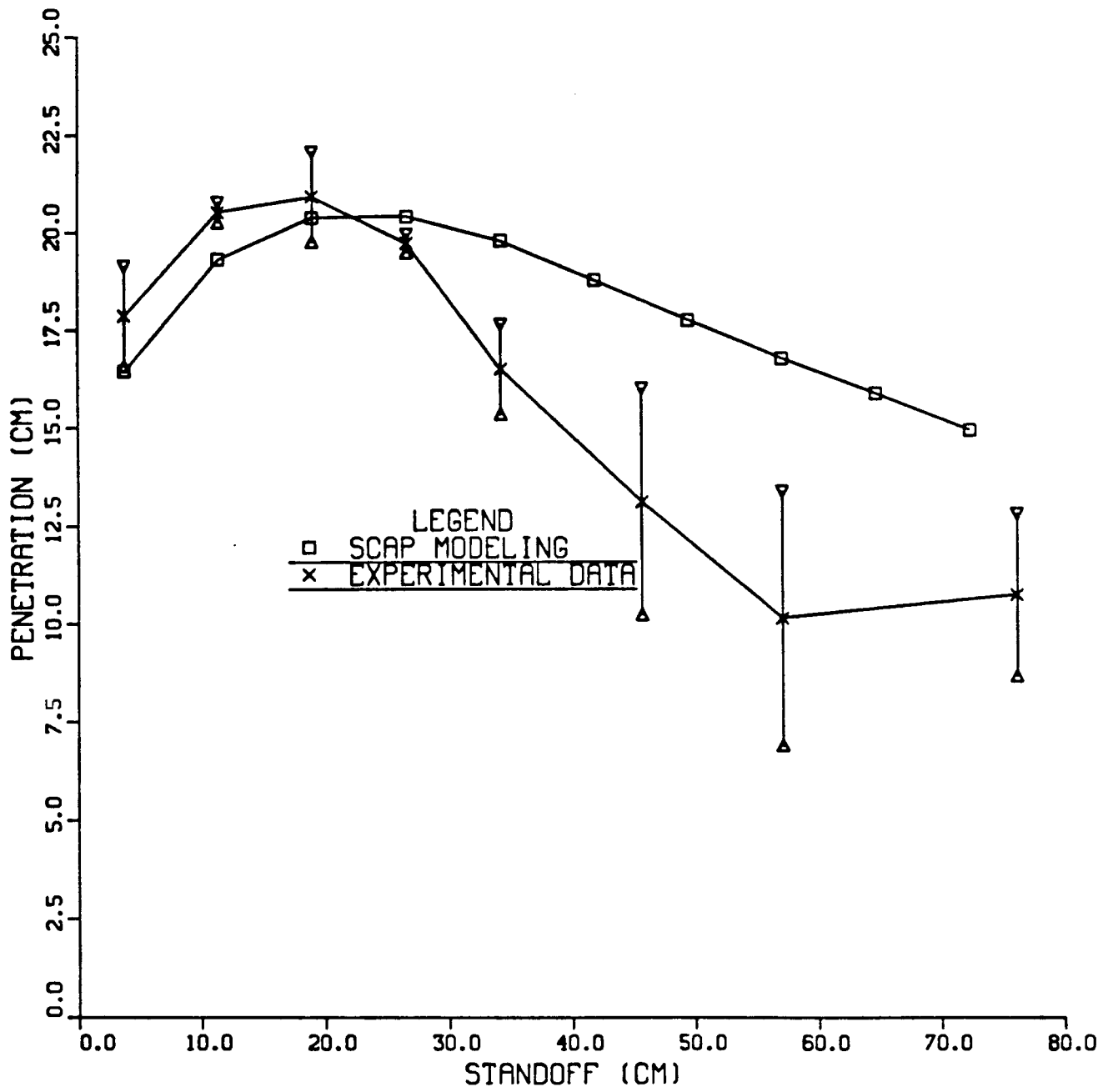


Figure 8. Penetration versus standoff for 20° copper liner and steel target.

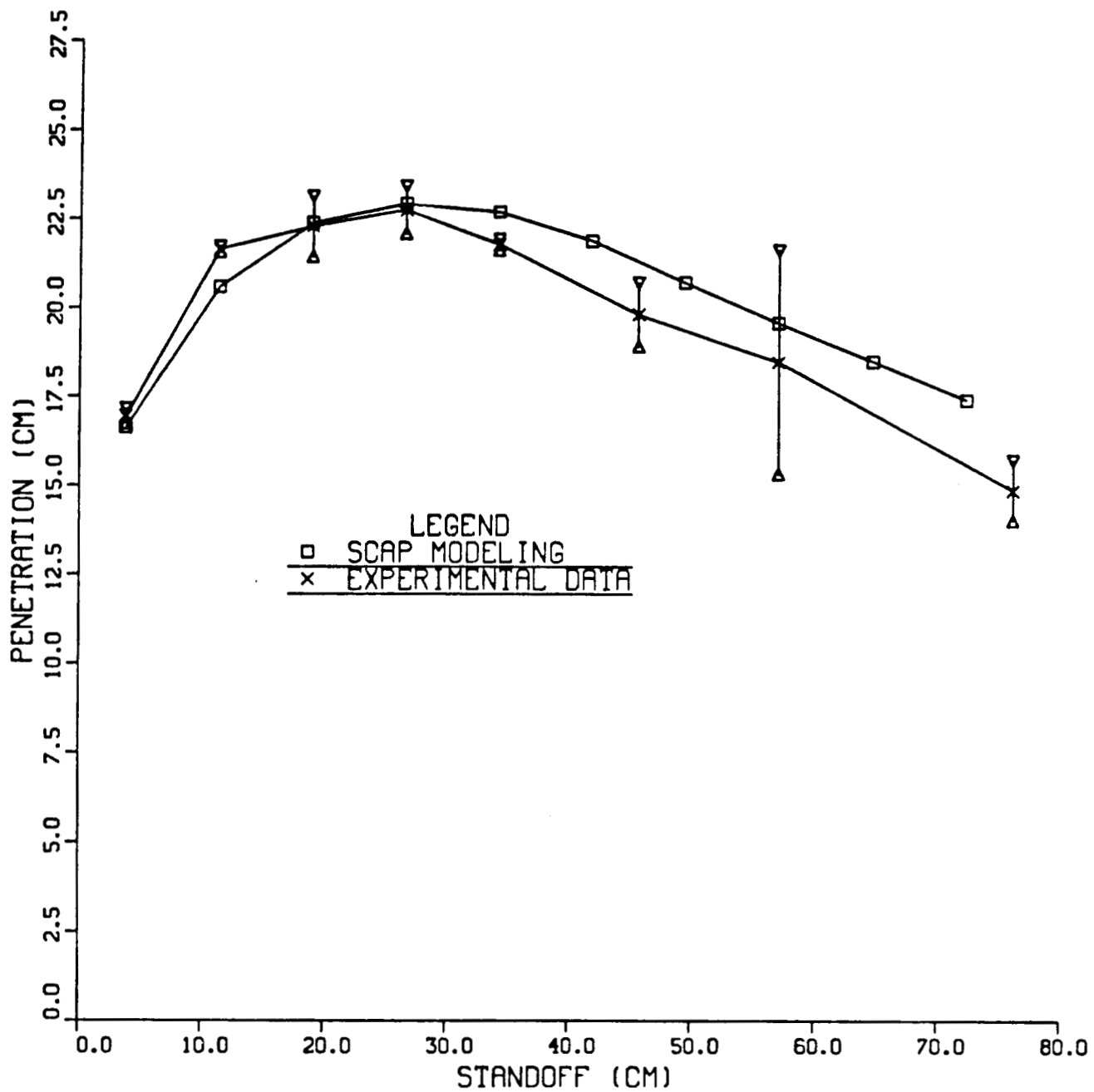


Figure 9. Penetration versus standoff for 40° copper liner and steel target.

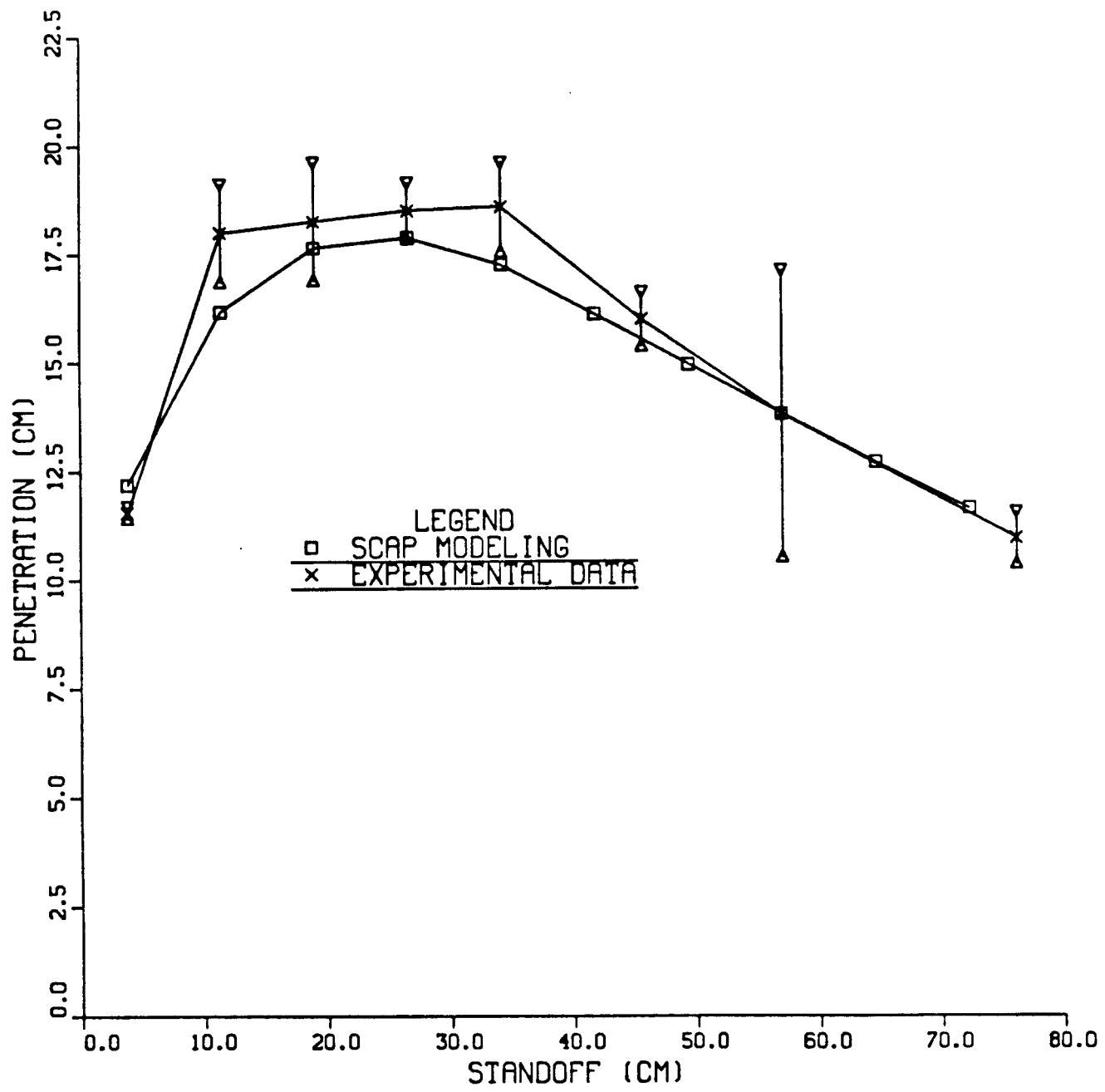


Figure 10. Penetration versus standoff for 60° copper liner and steel target.

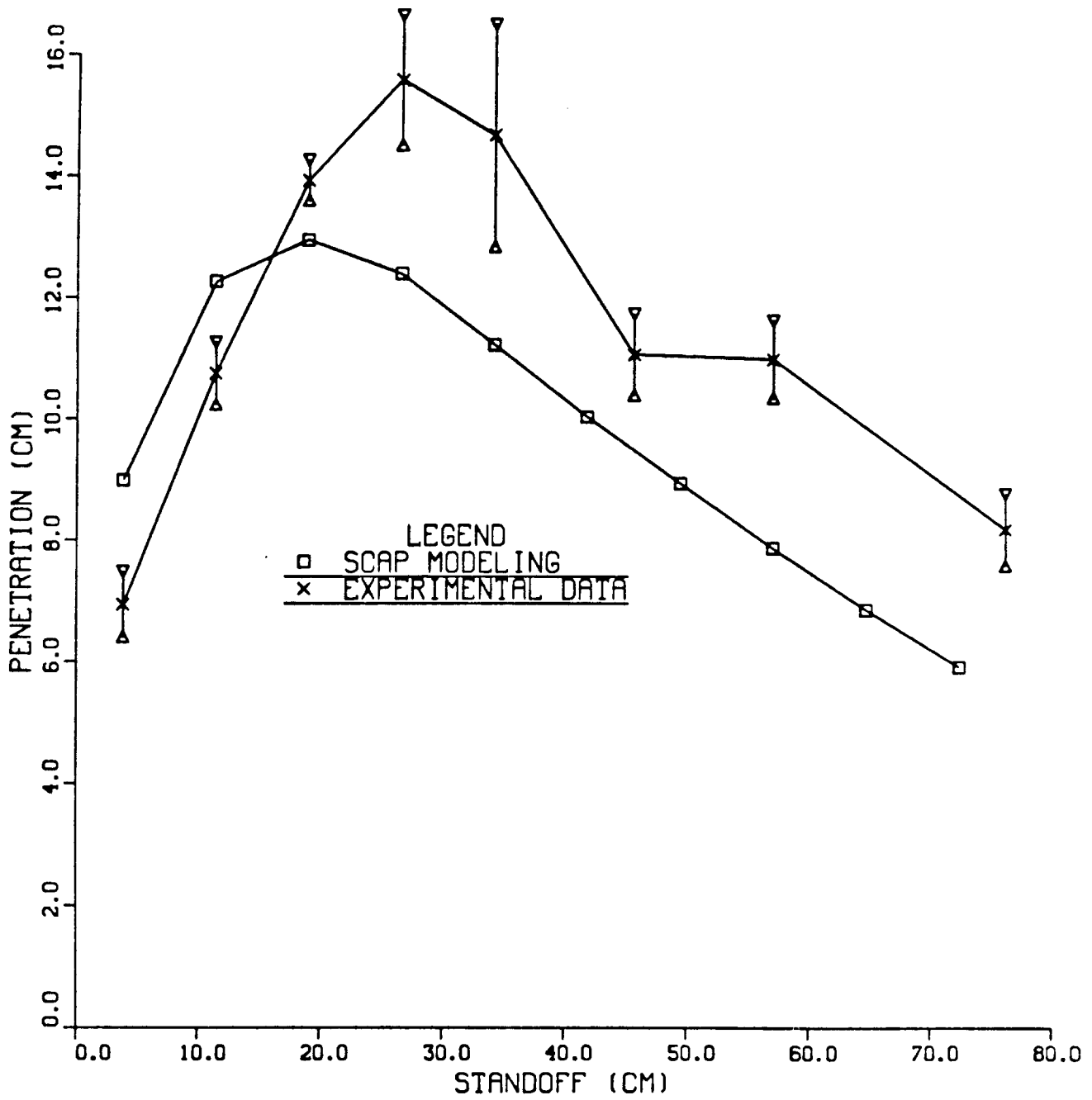


Figure 11. Penetration versus standoff for 90° copper liner and steel target.

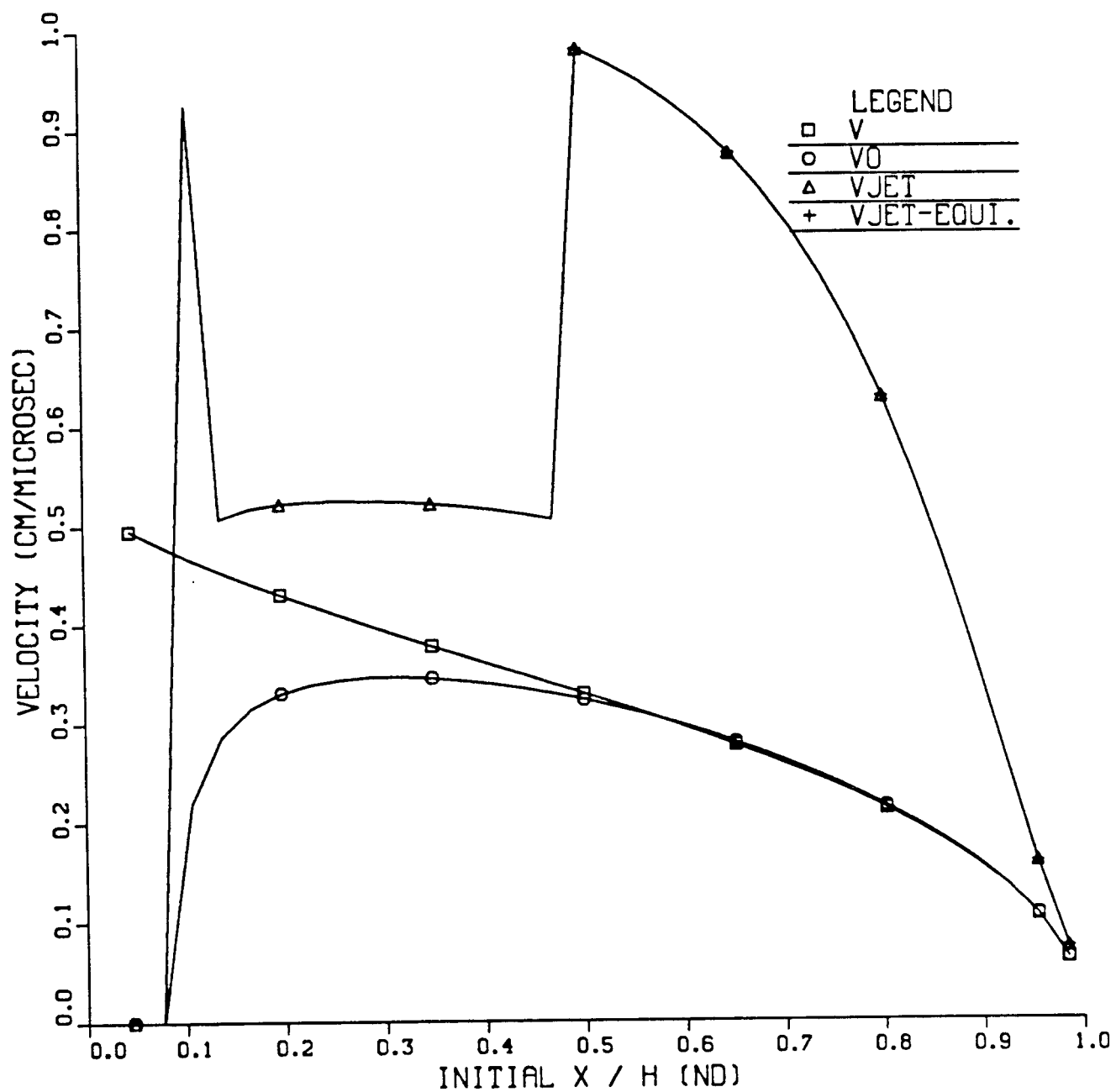


Figure 12. Velocities as a function of original axis position for 20° copper liner.

References

- 1. Allison, F. E. and R. Vitali.**
An Application of the Jet Formation Theory to a 105-mm Shaped Charge. *Ballistic Research Laboratories*, AD-277458, March 1962.
- 2. Austin, C. F.**
Lined Cavity Shaped Charges and Their Use in Rock and Earth Materials. Bulletin 69, State Bureau of Mines and Mineral Resources, New Mexico Institute of Mining and Technology, Socorro, NM, 1959.
- 3. Bertholf, L. D.**
Approximate Methods for Predicting Blast Pad Standoff Protection. *Sandia National Laboratories*, SAND83-8249, November 1983.
- 4. Birkhoff, G., D. P. MacDougall, E. M. Pugh and G. I. Taylor.**
Explosives with Lined Cavities. *J. Appl. Phys.*, **19**, June 1948, pp. 563-582.
- 5. Chou, P. C., J. Carleone and R. Karpp.**
Criteria for Jet Formation from Impinging Shells and Plates. *J. Appl. Phys.*, **47(7)**, July 1976.
- 6. Chou, P. C., E. Hirsch and R. D. Ciccarelli.**
An Unsteady Taylor Angle Formula for Liner Collapse. *Dyna East Corporation*, AD-A104682, 1981.
- 7. Chou, P. C., J. Carleone, W. J. Flis, R. D. Ciccarelli and E. Hirsch.**
Improved formulas for Velocity, Acceleration, and Projection Angle of Explosively Driven Liners. *Prop. Exp. Pyro.*, **8**, pp. 175-183, 1983.
- 8. de Boor, C.**
A Practical Guide to Splines. Applied Mathematical Science Vol. 27, Springer-Verlag, 1978.
- 9. DeFrank, P.**
Industrial Applications of Conical and Linear Shaped Charges. In *Behavior and Utilization of Explosives in Engineering Design*, Proceedings of the 12th Annual Symposium, New Mexico Section ASME, Albuquerque, New Mexico, March 1972, pp. 251-255.
- 10. DiPersio, R., J. Simon and A. B. Merendino.**
Penetration of Shaped-Charge Jets into Metallic Targets. *Ballistics Research Laboratories*, AD-476717, 1965.
- 11. DiPersio, R., W. H. Jones, A. B. Merendino and J. Simon.**
Characteristics of Jets from Small Caliber Shaped Charges with Copper and Aluminum Liners. *Ballistics Research Laboratories*, AD-823839, 1967.

12. **Harrison, J. T.**
Improved Analytical Shaped Charge Code: BASC. *Ballistic Research Laboratories*, AD-A100275, 1981.
13. **Jones, G. E., J. E. Kennedy and L. D. Bertholf.**
Ballistics Calculations of R. W. Gurney. *American Journal of Physics*, 48(4), April 1980, pp. 264-269.
14. **Kennedy, J. E.**
Gurney Energy of Explosives: Estimation of the Velocity and Impulse Imparted to Driven Metal. *Sandia National Laboratories*, SC-RR-70-790, December 1970.
15. **Kennedy, J. E.**
Explosive Output for Driving Metal. In *Behavior and Utilization of Explosives in Engineering Design*, Proceedings of the 12th Annual Symposium, New Mexico Section ASME, Albuquerque, New Mexico, March 1972, pp. 109-124.
16. **Pugh, E.M., R.J. Eichelberger and N. Rostoker.**
Theory of Jet Formation by Charges with Lined Conical Cavities. *J. Appl. Phys.*, 23(5), May 1952, pp. 532-536.
17. **Robinson, A. C.**
Asymptotic Formulas for the Motion of Shaped Charge Liners. *Sandia National Laboratories*, SAND84-1712, September 1984.
18. **Sedgwick, R. T., M. L. Gittings and J. M. Walsh.**
Numerical Techniques for Shaped Charge Design. In *Behavior and Utilization of Explosives in Engineering Design*, Proceedings of the 12th Annual Symposium, New Mexico Section ASME, Albuquerque, New Mexico, March 1972, pp. 243-250.
19. **Shear, R. E., F. S. Brundick and J. T. Harrison.**
A Link Between Shaped Charge Performance and Design. *Ballistic Research Laboratories*, AD-A106198, 1981.

Appendix A - Incremental Area between Two Curves

We describe the derivation of the incremental area or volume swept out by two curves parameterized by a single variable ξ . Let $\mathbf{x}_1(\xi)$ and $\mathbf{x}_2(\xi)$ be two curves in the plane oriented as in Figure 13, and let $\mathbf{x}(\xi, s) = (\mathbf{x}_2 - \mathbf{x}_1)s + \mathbf{x}_1$ with $0 \leq s \leq 1$ denote the line joining the points at a fixed ξ .

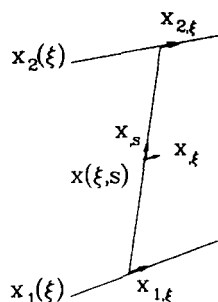


Figure 13. Incremental Area Vectors

In Figure 13, differentiation is denoted using subscripts. The incremental area between the curves is given by

$$\frac{dA}{d\xi} = \int_0^1 \frac{\partial \mathbf{x}}{\partial \xi} \wedge \frac{\partial \mathbf{x}}{\partial s} ds \quad (A.1)$$

where the integrand is the determinant of the Jacobian of the transformation $\mathbf{x}(\xi, s)$ or, equivalently, the magnitude of the cross product of the two vectors on either side of the \wedge symbol. The formula for incremental area is

$$\frac{dA}{d\xi} = \frac{d}{d\xi} \left(\frac{\mathbf{x}_1 + \mathbf{x}_2}{2} \right) \wedge (\mathbf{x}_2 - \mathbf{x}_1). \quad (A.2)$$

In cylindrical coordinates with $\mathbf{x}_1 = (x_1, r_1)$ and $\mathbf{x}_2 = (x_2, r_2)$, the incremental volume is given by the formula

$$\frac{dV}{d\xi} = 2\pi \int_0^1 r \frac{\partial \mathbf{x}}{\partial \xi} \wedge \frac{\partial \mathbf{x}}{\partial s} ds \quad (A.3)$$

where $r = (r_2 - r_1)s + r_1$. After evaluating the integral (A.3) one obtains

$$\frac{dV}{d\xi} = 2\pi \left(\left(\frac{r_2}{3} + \frac{r_1}{6} \right) \frac{d\mathbf{x}_2}{d\xi} + \left(\frac{r_2}{6} + \frac{r_1}{3} \right) \frac{d\mathbf{x}_1}{d\xi} \right) \wedge (\mathbf{x}_2 - \mathbf{x}_1). \quad (A.4)$$

Appendix B - Integrals of Acceleration Functions

B1: Impulsive Acceleration - Delta Function

$f = \delta(\eta)$ where δ is the initial value delta function defined by

$$\int_0^\eta \delta(s)g(s)ds = \begin{cases} g(0), & \eta > 0 \\ 0, & \eta \leq 0 \end{cases}$$

$$f_1 = \eta; \quad df_1/d\eta = \begin{cases} 1, & \eta > 0 \\ 0, & \eta \leq 0 \end{cases}$$

$$f_2 = 0; \quad df_2/d\eta = 0$$

$$f_3 = 0; \quad df_3/d\eta = 0$$

$$f_4 = \eta \int_0^\eta \int_0^s \delta(s)\delta(s')ds'ds = \eta/2; \quad df_4/d\eta = \begin{cases} 1/2, & \eta > 0 \\ 0, & \eta \leq 0 \end{cases}$$

B2: Exponential Acceleration

$$f = e^{-\eta}$$

$$f_1 = e^{-\eta} - (1 - \eta); \quad df_1/d\eta = 1 - e^{-\eta}$$

$$f_2 = (\eta + 1)e^{-\eta} + e^{-2\eta}/4 + \eta/2 - 5/4; \quad df_2/d\eta = -\eta e^{-\eta} - e^{-2\eta}/2 + 1/2$$

$$f_3 = (\eta + 2)e^{-\eta} - (\eta + 1)e^{-2\eta}/4 + 3\eta/4 - 7/4$$

$$df_3/d\eta = -(\eta + 1)e^{-\eta} + (\eta + 1/2)e^{-2\eta}/2 + 3/4$$

$$f_4 = e^{-\eta} - e^{-2\eta}/4 + \eta/2 - 3/4; \quad df_4/d\eta = -e^{-\eta} + e^{-2\eta}/2 + 1/2$$

B3: Constant Acceleration

$f(\eta) = H(\eta) - H(\eta - 1)$ where $H(\eta)$ is the Heaviside unit step function

$$f_1 = \eta^2 f(\eta)/2 + (\eta - 1/2)H(\eta - 1); \quad df_1/d\eta = \eta f(\eta) + H(\eta - 1)$$

$$f_2 = \eta^4 f(\eta)/24 + (\eta/6 - 1/8)H(\eta - 1); \quad df_2/d\eta = \eta^3 f(\eta)/6 + H(\eta - 1)/6$$

$$f_3 = \eta^4 f(\eta)/12 + (\eta/3 - 1/4)H(\eta - 1); \quad df_3/d\eta = \eta^3 f(\eta)/3 + H(\eta - 1)/3$$

$$f_4 = \eta^3 f(\eta)/6 + (\eta/2 - 1/3)H(\eta - 1); \quad df_4/d\eta = \eta^2 f(\eta)/2 + H(\eta - 1)/2$$

B4: Modified Exponential Acceleration

$$f = (1 + \eta)e^{-\eta}/2$$

$$f_1 = (2\eta - 3 + (\eta + 3)e^{-\eta})/2$$

$$df_1/d\eta = (2 - (\eta + 2)e^{-\eta})/2$$

$$f_2 = (22\eta - 73 + (16\eta^2 + 56\eta + 56)e^{-\eta} + (2\eta^2 + 12\eta + 17)e^{-2\eta})/32$$

$$df_2/d\eta = (11 - (8\eta^2 + 12\eta)e^{-\eta} - (2\eta^2 + 10\eta + 11)e^{-2\eta})/16$$

$$f_3 = (35\eta - 109 + (16\eta^2 + 80\eta + 128)e^{-\eta} - (2\eta^3 + 12\eta^2 + 25\eta + 19)e^{-2\eta})/32$$

$$df_3/d\eta = (35 - (16\eta^2 + 48\eta + 48)e^{-\eta} + (4\eta^3 + 18\eta^2 + 26\eta + 13)e^{-2\eta})/32$$

$$f_4 = (16\eta - 35 + (16\eta + 48)e^{-\eta} - (2\eta^2 + 10\eta + 13)e^{-2\eta})/32$$

$$df_4/d\eta = (4 - (4\eta + 8)e^{-\eta} + (\eta^2 + 4\eta + 4)e^{-2\eta})/8$$

Appendix C - Code Structure, Subroutines and Variables

C1: Code Structure

SCAP is structured to provide an easy to use format for the the shaped charge designer to develop his specific components. All geometrical and physical data may be input interactively. This information is saved for future use in a file with format given in Appendix D. Several modeling options are available in the code. These are chosen by default or may be chosen interactively by the user. The code is designed to run with a minimum of input by the user. Modeling and output options may be explored by the user as interest and need requires.

SCAP is written in Fortran 77 and uses many of the new FORTRAN features. The code has been developed for use on VAX systems at Sandia but should be easily adaptable to other computer systems. The commercial plotting package, DISSPLA, is used by the code. The Sandia SLATEC mathematical subroutine library is also accessed.

The coding occurs in the following sequential order: initialization, geometrical computations necessary for the explosive and acceleration modeling, computation of acceleration parameters along the liner and confinement, liner motion and jet and slug formation, jet virtual origin calculation, jet breakup, and target penetration. Printing and plotting output code typically follows immediately after the corresponding modeling coding. A final section computes jet stretching and plots and/or prints at previously specified times. This last section may be used to make movies of the modeled shaped charge jetting process.

The code is independent of units so that any self-consistent set of units in the input data may be used. The system of units composed of grams (gm), centimeters (cm) and microseconds (μ sec) is convenient for shaped charge applications. In this case, the Mbar is the derived unit of stress.

Appendix C2 lists SCAP subroutines. DISSPLA and VAX system routines are not included. Appendix C3 defines arrays and variables. Appendix C4 lists variables in FORTRAN COMMON and values of PARAMETER constants.

C2: SCAP Subroutines

Routine	Function
INTERP	Interpolation Routines - Uses quadratic or not-a-knot cubic spline. (See deBoor (1978)). Interpolant is returned in piecewise cubic form.
DADXI	Computes incremental volume change between two curves parameterized by a single variable. See Appendix A.
CCHANGE ICHANGE RCHANGE	Interactive modification of character, integer and real variables, respectively.
CUBEVAL	Evaluates at a point a specified derivative of piecewise cubic polynomial representation of a function.
DERKF	Ordinary differential equation solver in SLATEC library.
LEFTJ	Left justify a character variable.
PVEL	Computes penetration velocity (g in equation (7.1)).
RLIN	Liner geometry. Entry point RLIN1 computes surface of exposed side of liner as a function of $\xi \in [0, 1]$. Entry point RLIN2 computes surface of explosive side of liner as a function of $\xi \in [0, 1]$.
RCON	Confinement geometry. Entry point RCON1 computes radius of explosive side of tamper as a function of $x \in [XDET, H]$. Entry point RCON2 computes radius of exposed side of confinement as a function of $x \in [XDET, H]$.
VELGR	Adjusts jet or slug velocity using inelastic collision model. If GRADFLAG is true (false), output velocity is nondecreasing (nonincreasing) with respect to ξ .
ZXT	Computes z , $\partial z/\partial t$ and $\partial z/\partial \xi$ as a function of ξ , z_0 , θ_0 , τ , V , T and their ξ derivatives from equations 4.7 and 4.8. Acceleration function f chosen according to flag IACCEL.

C3: Definition of Variables

Array	Definition	Symbol
ALPHAC(NMAX,2)	Initial confinement angle	α
AMDC(NMAX,2)	Projection direction for confinement	$\alpha - \delta$
BETA(NMAX)	Liner angle at axis	β
DELTAC(NMAX,2)	Confinement projection angle	δ
DMCON(NMAX,2)	Incremental confinement mass	M
DMEXP(NMAX,2)	Incremental explosive mass	C
DMJET(NMAX)	Incremental jet mass	dm_j
DMLIN(NMAX)	Incremental liner mass	$dm_{l,N}$
DMSLG(NMAX)	Incremental slug mass	dm_s
DZLIN(NMAX)	Vector used for plotting purposes—complex	
IFORM(20)	Integer array for DISSPLA plot titles	
INFO(15)	Flag array used by DERKF	
IPAR(10)	Parameter array used by DERKF and PVEL	
IPKRAY(500)	Integer array for DISSPLA legends	
IWORK(33)	DERKF work array	
OUT _m (NMAX)	Temporary arrays for output. $m = 1, \dots, 6$	
P(NPMAX)	Penetration array	
PEN(NSOFFMAX)	Penetration-standoff array	
RC1(NMAX)	Initial inner face of confinement	
RC2(NMAX)	Initial free face of confinement	
RCC(NLCMAX)	Coefficients for routine RCON	
RJET(NMAX)	Radius of jet	r_j
RLC(NLCMAX)	Coefficients for routine RLIN	
RPAR(10)	Parameter array used by DERKF and PVEL	
RSLG(NMAX)	Radius of slug	
RWORK(40)	Temporary array for DERKF	
SOFF(NSOFFMAX)	Standoff values	
SPL _m (4,NMAX)	Temporary arrays for interpolation data.	
SPL _{nX} (4,NMAX)	SPL(i,j) gives (i-1)st derivative at point j. $m = 1, \dots, 9$. $n = 1, 2$	

Array	Definition	Symbol
TARGET (NTARMAX,8)	Target parameter array	
TAU(NMAX)	Acceleration time	τ
TBREAK(NMAX)	Jet breakup time	t_b
TDETRC(NMAX,2)	Time detonation arrives at confinement	
TDETRL(NMAX,2)	Time detonation arrives at liner	T
TLAXIS(NMAX)	Time liner element arrives at axis	t_a
TOUT(NTOUT)	Specific times for snapshot output	
TP(NPMAX)	Penetration times corresponding to P array	
TPEN(NSOFFMAX)	Penetration termination times vs. standoff	
V(NMAX)	Liner velocity. See equations (4.1,4.5).	V
VCON(NMAX,2)	Velocity of confinement	V_c
VF(NMAX)	Flow velocity in collapse point frame	V_f
VJET(NMAX)	Jet element velocity	V_j
VSLG(NMAX)	Slug element velocity	V_s
VSP(NMAX)	Collapse point velocity	V_{sp}
XAXIS	X collapse point for liner element	x_a
XC(NMAX)	Array for initial confinement plotting	
XCDET(NMAX,2)	Confinement zoning array	
XJET(NMAX)	X location of jet element	x_j
XLM(NMAX,2)	Zone centered values of ξ	ξ
XP(NMAX)	X position of penetration points P	x_p
XPEN(NSOFFMAX)	Total penetration x location vs. standoff	
XSLG(NMAX)	x location of slug element	x_s
	XJET,XSLG,RJET,RSLG also contain liner positions for plotting purposes.	

Variable	Definition	Symbol
A	See equation 2.3	A
AIC	Angle used in confinement motion	
ATOL	Absolute error tolerance for DERKF	
B	See equation 2.3	B
CUTJET	Cutoff ratio for V_f/c	κ
CVIR	Correlation coefficient for virtual origin computation	
DATETIME	Date and time - character*24	
DCON	Confinement density	
DEXP	Explosive density	
DIS	Distance from detonation point to detonation front on liner	
DLIN	Liner and jet density	ρ_j
DX	Incremental ξ or x	
DX1	Incremental x for $x < 0$	
DX2	Incremental ξ	
DZDT	Liner element velocity vector - complex	$\partial z/\partial t$
DZDXI	Liner element tangent vector - complex	$\partial z/\partial \xi$
ETOL	Error tolerance used in iterations - Parameter constant	
ETYPE	explosive type - Character*10	
F	See equation 4.3	F
FLAG	I/O flag - Character*1	
FORM	Variable for format creation - Character*400	
GAMMA	Coefficient of expansion for explosive	γ
H	Length from top of liner to base	
HDET	Distance from liner base to detonation point	
IACCEL	Acceleration function indicator	
LAXIS	Collapse point modeling flag	
IBREAK	Jet breakup modeling flag	
ICS	Internal indicator for removing inconsistent zones near detonation point	
IDETCON	Flag for position of det. front on confinement	
IDETLIN	Flag for position of det. front on liner	
IDID	DERKF return flag	
IFILE	File name length indicator in I/O processing	

Variable	Definition	Symbol
Igeom	Geometry indicator (=1,2)	
IGURZONE	Indicator for zoning option	
IINTER	Interpolation type flag	
IJET	Zone number for first jet element	
INFILE	Name of input file	
IPDETAIL	Single standoff for detailed penetration output	
IPEN	Total number of DERKF integration steps	
IPMAX	Standoff number of maximum penetration	
ISHADE	Flag for DISSPLA shading type	
ISIMDET	Simultaneous or sweeping detonation flag	
ISOFF	Current standoff number	
ITIME	Time snapshot flag	
LJET	Last element in jet	
LC,NLC	Length, mass, time, velocity and kinetic energy	
MC,NMC	titles in characters variables and the	
TC,NTC	associated length of the character titles.	
VC,NVC		
KC,NCK		
MOVIE	Flag for fixed frame size-logical	
N	NZ+1	
NC	Number of coefs. in confinement definition	
NL	Number of coefs. in liner definition	
NLCMAX	Maximum value allowed for NC or NL - Parameter constant	
NMAX	Dimension of liner arrays. $NMAX \geq N$ - Parameter constant	
NMAX2	$2*NZ$ - Parameter constant	
NPMAX	Maximum number of penetration integration steps - Parameter constant	
NPP	Number of output times	
NSOFFMAX	Maximum number of standoffs - Parameter constant	
NTARMAX	Maximum number of target layers - Parameter constant	
NTOUT	Maximum number of separately specified snapshot times- Parameter constant	
NZ	Number of zones in $\xi > 0$ and in $x < 0$	

Variable	Definition	Symbol
OUTFILE	Hardcopy of output filename	
PDETAIL	Detailed penetration plots flag - Logical	
PI	Constant	
PLOT	Flag for plotting - Logical	
PRINT	Flag for printout - Logical	
RDET	Radius of detonation point	
REXP	Thickness of explosive in Gurney modeling	d_0
RT2E	Gurney velocity	$\sqrt{2E}$
RTOL	Relative error tolerance for DERKF	
SOFFMAX	Maximum standoff	
SOFFMIN	Minimum standoff	
T	Current time	t
TB	Jet breakup time from detonation initiation	t_b
T1	Jet breakup time from virtual time origin	t_1
TIMEINT	Time interval between print and/or plot output	
TKEJET	Total kinetic energy of jet	
TMCON	Total confinement mass	
TMEXP	Total explosive mass	
TMJET	Total jet mass	
TMLIN	Total liner mass	
TMSLG	Total slug mass	
TVIR	Jet virtual time origin	t_0
VARG	Velocity direction at collapse	$\arg(\frac{\partial z}{\partial t})$
VBLKL	Bulk sound speed of liner material	c
VDET	Explosive detonation velocity	
VMAG	Velocity magnitude at collapse	V_0
X, Y	Laboratory coordinates	x, y
XDET	Axis position of detonation point (< 0) $XDET = H - HDET$	
XMIN,XMAX	Used for axis setup in plotting	
XSOFF	X position of target face	
XVIR	Jet virtual axis origin	x_0
XYFAC	Overall scaling factor for plotting	
YCLPS	Value of radius identified with collapse of liner	y_{clps}
YLIN	Dynamic yield stress for jet material	
YMAX	Used for axis setup in plotting	
Z	Location of liner element - Complex	z

C4: COMMON Blocks and PARAMETER Constants

The COMMON blocks and associated variables used in SCAP are

COMMON Block	Variable list
COMMON/INTERCOM/	IINTER
COMMON/RCOM/	NL, RLC, NC, RCC, XDET, H
COMMON/TARCOM/	TARGET, XLM, SPL6, SPL7, SPL8, SPL9

Note that all common variables are arrays except for IINTER, NL, NC, XDET and H.

The values of PARAMETER constants and their current numerical values as defined in the SCAP source code are

Constant	Value
NMAX	100
NMAX2	200
NLCMAX	20
ETOL	1.E-5
NPMAX	1000
NTARMAX	10
NSOFFMAX	20
NTOUT	20

Appendix D - Input and Output

Two basically different types of input are needed for running SCAP. First, basic physical and geometrical data are needed to set up the charge configuration. These may be input interactively and are then stored on disk file for further use as an input file. Alternatively, the input file may be created with a text editor. The input deck may also be altered and saved while in the initialization portion of the code.

The second type of input consists of modeling and output options. These may be specified interactively at run time, if other than default options are desired. The default options may also be easily modified in the code if desired.

Modeling parameters and modeling default options are changed in the code by calls to subroutines CCHANGE, ICHANGE and RCHANGE for character, integer and real variables, respectively. These three routines type a description of the parameter along with its current value to the user's terminal and wait for a response. A single carriage return will leave the parameter unaltered and the program will continue. If the user inputs a value and then follows with a carriage return, the old value will be replaced and the routine will display the new value for a double check. Once a single carriage return is received, the program will proceed with the new value.

The input file consists of a minimum of 8 sequential lines in a text file. This file is denoted *name*.DAT where *name* has a maximum of nine characters. The file contains the appropriate information in the specified fields as given in the table on the following page. In the units column of the table, mass, length and time units are reference by M, L, and T, respectively. All angles are in degrees. Unless specified as a character variable, the variable type for the input follows default FORTRAN conventions according to first letter where (A-H,O-Z) indicates a real FORTRAN variable and (I-N) indicates an integer variable. The integer variable must be right justified in the field, and the real variables should contain a decimal point within the field. The real variables may or may not contain an exponent, but if an exponent is used, the variable must be right justified in the field.

Line	Field	Variable	Description	Units
1	(1 -10)	MC	Mass units - Character*10	-
	(11-20)	LC	Length units - Character*10	-
	(21-30)	TC	Time units - Character*10	-
2	(1 - 5)	IGEOM	Geometry flag-Linear=1; Conical=2	-
	(6 -10)	NZ	Number of zones	-
			If blank, code will compute NZ	-
	(11-20)	ETYPE	Explosive type - Character*10	-
	(21-30)	DEXP	Explosive density	M/L**3
	(31-40)	VDET	Detonation velocity	L/T
	(41-50)	RT2E	Gurney velocity = $\sqrt{2E}$	L/T
	(51-60)	GAMMA	Explosive adiabatic expansion coef.	-
3	(1 -10)	DLIN	Density of liner	M/L**3
	(11-20)	VBLKL	Bulk sound speed of liner	L/T
	(21-30)	CUTJET	Cutoff ratio, κ , for jetting	-
	(31-40)	TB	Jet breakup time from	T
			detonation initiation	
	(41-50)	T1	Jet breakup time from virtual origin	T
	(51-60)	YLIN	Dynamic yield stress for jet	M/(LT**2)
			Note: Only one of TB,T1 and YLIN is used depending on the jet breakup modeling option chosen.	
(61-70)	NL	Number of coefficients describing liner geometry (=3 or 4)	-	
4	(1 -10)	RLC(1)	Inner liner cone half angle	deg
	(11-20)	RLC(2)	Inner liner y intercept at base	L
	(21-30)	RLC(3)	Liner thickness (NL=3)	L
			Outer liner cone half angle (NL=4)	deg
	(31-40)	RLC(4)	Outer liner y intercept at base (NL=4) See line 7 for truncated apex option.	L
5	(1 -10)	DCON	Confinement or tamper density	M/L**3
	(11-20)	NC	Number of coefficients describing tamper geometry (= 3,4 or 8)	-

Line	Field	Variable	Description	Units
6	(1-10)	RCC(1)	Explosive side tamper angle	deg
	(11-20)	RCC(2)	Explosive side tamper y intercept at base	L
	(21-30)	RCC(3)	Tamper thickness (NC=3)	L
			Outer tamper angle at base(NC=4,8)	deg
	(31-40)	RCC(4)	Outer tamper y intercept at base (NC=4,8)	L
	(41-50)	RCC(5)	Axial distance from base to inner tamper slope change (NC=8)	L
	(51-60)	RCC(6)	Axial distance from base to outer tamper slope change (NC=8)	L
	(61-70)	RCC(7)	Inner tamper angle after slope change (NC=8)	deg
	(71-80)	RCC(8)	Outer tamper angle after slope change (NC=8)	deg
7	(1-10)	HDET	Distance from detonation x point to base	L
	(11-20)	RDET	Detonation y point. RDET $\neq 0$ indicate ring detonation	L
	(21-30)	H	Exterior x dimension of liner (Apex to base) Must not be greater than virtual apex distance defined implicitly by line 4 data. If blank, code sets to virtual apex; if nonzero, cone apex will be truncated at height H.	L
	(31-40)	SOFFMIN	Minimum standoff of interest	L
	(41-50)	SOFFMAX	Maximum standoff of interest	L
	(51-60)	NSOFF	Total number of target standoffs	-
	(61-70)	NTL	Total number of target layers	-
	8	(1-10)	TARGET(*,1)	Target layer density.
(11-20)		TARGET(*,2)	Target layer thickness	L
(21-30)		TARGET(*,3)	Minimum penetration velocity for layer	L/T
(31-40)		TARGET(*,4)	Coefficient in dynamic yield stress jet breakup model. In a future version of SCAP this will probably be the target hole size coefficient.	-

Line 8 is repeated NTL times.

The following is a sample input deck which we shall call DJMS1B.DAT

```

GRAM      CM      MICROSEC
  2      0      COMP B 1.720E+00  7.980E-01  3.000E-01  2.850E+00
8.940E+00 3.920E-01 1.230E+00  0.000E+00  6.390E+01  2.000E-03      3
2.000E+01 1.781E+00 1.168E-01
7.850E+00      3
0.000E+00 1.905E+00 4.763E-01
1.082E+01 8.000E-01 0.000E+00  3.810E+00  7.239E+01      10      1
7.850E+00 1.000E+04 1.600E-01  5.400E+00

```

Modeling options may be chosen interactively at run time if requested by the user. Otherwise default modeling options are taken. Current options include:

Model	Flag	Options
Gurney acceleration	IACCEL	1=Impulsive acceleration 2=Exponential fit 3=Constant fit 4=Modified exponential fit (default)
Collapse point	IAXIS	1 = radius at collapse equal zero 2 = ad hoc model (See eq. (4.15)) (default)
Jet breakup	IBREAK	1 = breakup time equals TB (default) 2 = breakup time equals $t_0 + T1$ 3 = dynamic yield stress model
Gurney zoning	IGURZONE	1=Radial zones (default) 2=Detonation front zoning
Interpolation	IINTER	2=Quadratic (default) 3=Not-a-knot cubic spline (See deBoor (1978))
Detonation	ISIMDET	1=Point or ring initiation 2=Simultaneous initiation (Default = 3 - IGEOM)

Suppose the input file name is *name.DAT*. After run completion, hardcopy output will be found in *name.LIS*. Plotting output will depend on the output mode chosen at link time. Any output device supported by DISSPLA in conjunction with the Sandia Virtual Device Interface (SVDI) is acceptable. Default output is for creation of both a *name.LIS* file and for standard plotted output. Several options for extended output and for fixing plotting scales are available interactively at run time by entering the output options portion of the code.

An important additional feature of the code permits simultaneous display of user data (e.g. from experiments) with modeling computations. User data for a given plot must be in the user's current directory in files *name.VJX*, *name.PT*, *name.PX*, *name.PS* and *name.CVX* where *name.DAT* is the input file name. The table on page 56 describes the contents of each of the above files. The format for these data files is given below. The first line in the data files gives the number of lines containing points to be plotted. The points are then found on subsequent sequential lines with abscissa then ordinate on a single line separated by at least one blank character. For files *name.PX* and *name.PT* this sequence is repeated for each standoff to be plotted. If no data is available for a given standoff a single line with a zero entry is needed. An important exception to this format is the penetration-standoff curve input file, *name.PS*. In this case the first line contains three values: the number of points, an abscissa scaling factor, and an ordinate scaling factor. The subsequent lines contain the abscissa, the ordinate and the experimentally observed deviation on either side of the ordinate (e.g. a $1-\sigma$ value). Both the ordinate and the deviation will be scaled by the ordinate scaling factor. The deviation values may be zero. These data files need not be present for SCAP to run. However, SCAP will always look for these files in the user's current directory and try to plot from them if they are found.

A sample data file, DJMS1B.PS, is given below and may be compared with output on page 65.

8	3.81	2.54
1.0	6.67	0.08
3.0	8.52	0.03
5.0	8.77	0.33
7.0	8.95	0.26
9.0	8.57	0.06
12.0	7.80	0.35
15.0	7.28	1.24
20.0	5.87	0.33

The program uses FORTRAN unit numbers 50 through 54 to read the experimental data files. Unit 10 is used for other SCAP file input and output purposes. Unit numbers 8, 55, 77 and 78 are reserved for plotting purposes. Unit numbers 5 and 6 are the user terminal input and output unit numbers, respectively. A table of program files, input files and output files (files created during the run) follows:

File	Description
<i>name</i> .DAT	Input file containing physical and geometrical data
<i>name</i> .LIS	Output listing file
FOR008.DAT	DISSPLA message file: not usually of interest
<i>name</i> .VJX	Data file: Jet velocity vs. original axis location
<i>name</i> .PT	Data file: Penetration vs. time from initiation
<i>name</i> .PX	Data file: Penetration vs. original axis location
<i>name</i> .PS	Data file: Penetration vs. standoff
<i>name</i> .VCX	Data file: Tamper velocity vs. original axis location
FOR055.DAT	Plot output file using SVDI metafile (MET) output device. The VAX POST utility is used for further processing. For information type \$SHELP DISS UTIL POST
FOR077.DAT	Device codes for VAX queued plotting devices will produce this file. The file must be sent to the output queue. See your system manager for details.
SCAP.FOR	Main SCAP FORTRAN source file
SCAP.OBJ	Compiled SCAP object code
SCAP.EXE	Usual name for executable file created after linking SCAP.OBJ with the SLATEC library and DISSPLA with a specific plotting device code. The executable file must correspond to the user's output plotting device!

Appendix E - Sample Run Sequence

The following describes a sample input sequence for a Sandia VAX computer configuration. We assume the main FORTRAN source code, SCAP.FOR, the input files, DJMS1B.DAT and DJMS1B.PS, are found in the user's current VAX directory. We also assume that all necessary plotting and subroutine library symbols have been defined by executing the commands

```
$OSYS$PSYMS: GRAPHSYMS  
$OSD: [MATHLIB] MATHSYMS
```

These commands should be placed in the user's LOGIN.COM file in his main directory so that the symbols will be defined automatically at login time. To compile and link SCAP the user executes the following sequence of commands:

```
$FORTRAN SCAP  
$LINK SCAP, SLATEC/LIB, 'LINK_DISS', 'LINK_xxx'
```

where **xxx** is the device code for your plotting device. A list of some, but not necessarily all valid device codes, can be obtained by typing

```
$SHELP DISS DEVICES
```

The object and executable files, SCAP.OBJ and SCAP.EXE, are created by the FORTRAN and LINK commands respectively. Once the executable file is created, for a given plotting device, the user need not repeat the above sequence with each run.

The following shows a sample user input sequence for running SCAP. The case chosen is a 40° liner apex angle charge of DiPersio, et. al (1967) discussed in Section 8. All default modeling options were chosen except for the jet breakup modeling since the virtual origin breakup time was available in this case. Several non-default output options were also selected. In the following, (cr) indicates carriage return from the user terminal.

```
$ RUN SCAP  
You are now running SCAP, the shaped charge
```

analysis program of Sandia National Laboratories.
 Instructions for getting the input deck and choosing
 modeling and output options will follow before
 proceeding with the computation. Requests requiring
 input data will be repeated until a return is given
 signifying that the input is correct.

Input file name = name.DAT => DJMS1B.DAT (cr)
 Input file name = DJMS1B.DAT => (cr)

MASS	LENGTH	TIME						
GRAM	CM	MICROSEC						
IGEOM	NZ	ETYPE	DEXP	VDET	RT2E	GAMMA		
2	30	COMP B	0.172E+01	0.798E+00	0.300E+00	0.285E+01		
	DLIN	VELKL	CUTJET	TB	T1	YLIN	NL	
	0.894E+01	0.392E+00	0.123+01	0.000E+00	0.639E+02	0.200E-02	3	
LINER PARAMETERS								
	0.200E+02	0.178E+01	0.117E+00					
	DCON	NC						
	0.785E+01	3						
CONFINEMENT PARAMETERS								
	0.000E+00	0.190E+01	0.476E+00					
	HDET	RDET	H	SOFFMIN	SOFFMAX	NSOFF	NTL	
	0.108E+02	0.800E+00	0.523E+01	0.381E+01	0.724E+02	10	1	
	DTAR	THICK	UMIN	HOLEC				
	0.785E+01	0.100E+05	0.16E+00	0.540E+01				

Do you wish to revise the input deck? (=Y)
 (cr)

Do you wish other than default modeling options? (=Y)
 Y(cr)

***** MODELING MENU *****

* ACCELERATION *

GURNEY ACCELERATION

- IMPULSIVE ACCELERATION = 1
- EXPONENTIAL FIT (EXP(-S)) = 2
- CONSTANT FIT = 3

- (1+S)*EXP(-S)/2. = 4

IACCEL = 4 =>(cr)

* ACCELERATION *

GURNEY ZONING

- RADIAL ZONES = 1

- DETONATION FRONT ZONING = 2

IGURZONE = 1 =>(cr)

* JET COLLAPSE POINT *

COLLAPSE ON AXIS (YCLPS=0) = 1

OFF AXIS AD HOC MODEL (YCLPS > 0) = 2

IAXIS = 2 =>(cr)

* INTERPOLATION TYPE *

QUADRATIC INTERPOLATION = 2

NOT-A-KNOT CUBIC SPLINE = 3

IINTER = 2 =>(cr)

* DETONATION MODELING *

POINT DET. AT (XDET,RDET) = 1

SIMULTANEOUS = 2

ISIMDET = 1 =>(cr)

* JET BREAKUP MODELING *

ABSOLUTE BREAKUP TIME GIVEN = 1

BREAKUP TIME RELATIVE TO VIRTUAL ORIGIN = 2

DYNAMIC YIELD STRESS MODEL = 3

IBREAK = 1 =>2

IBREAK = 2 =>(cr)

END OF MODELING MENU

Do you wish other than default output options? (=Y)

Y

**** OUTPUT MENU ****

* PRINT/PLOT TIME SNAPSHOTS AT *

- REGULAR INTERVALS = 1

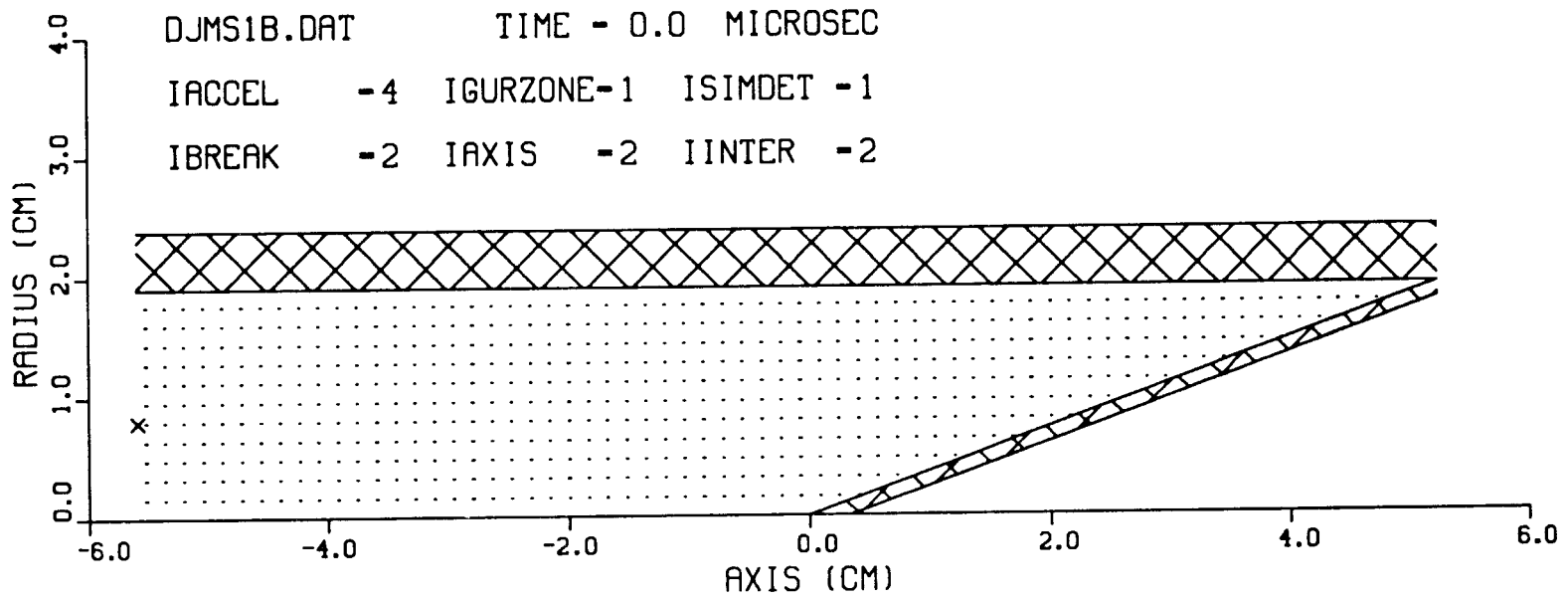
- SPECIFIC TIMES = 2

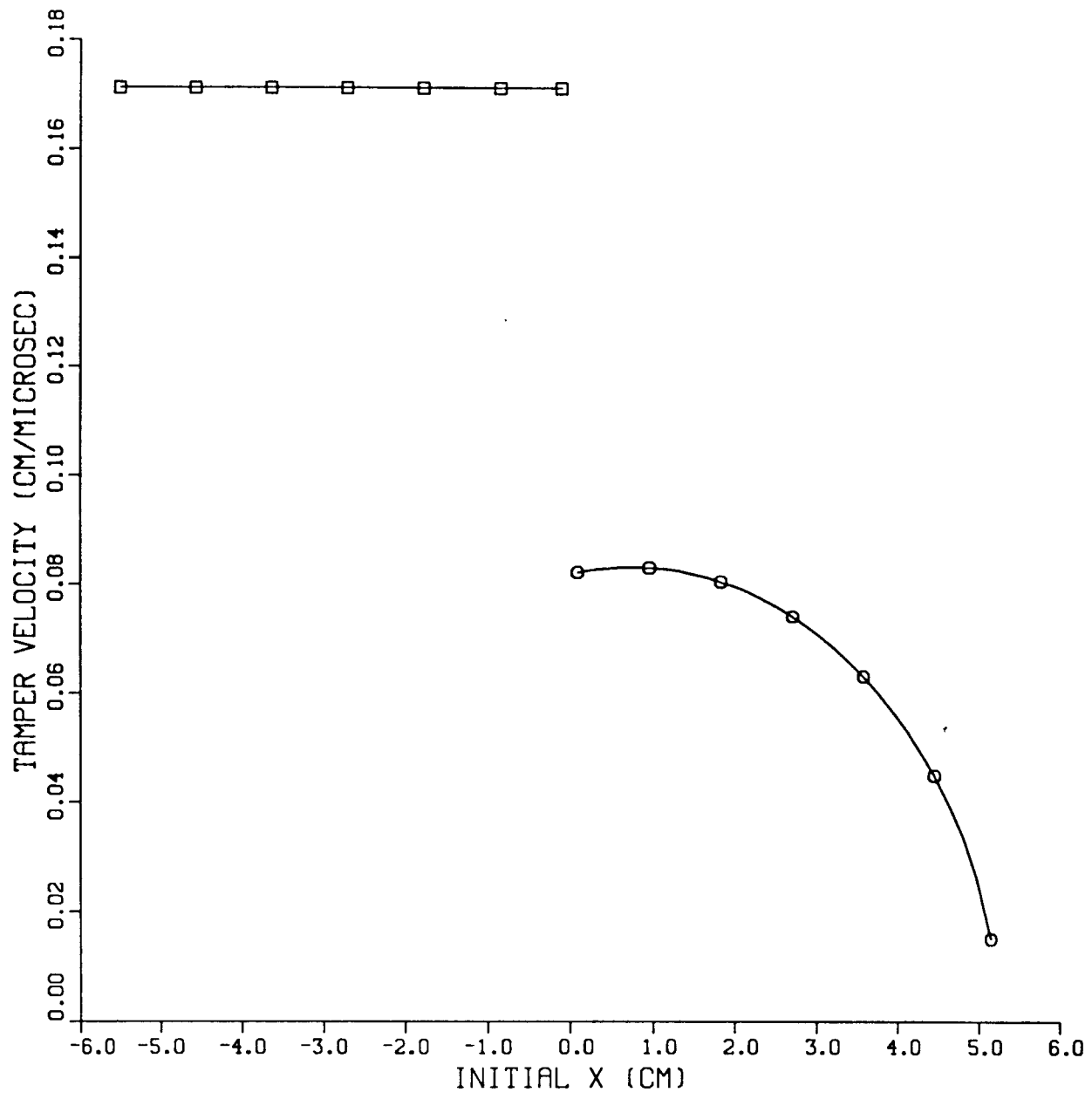
- NO SNAPSHOT OUTPUT = 3

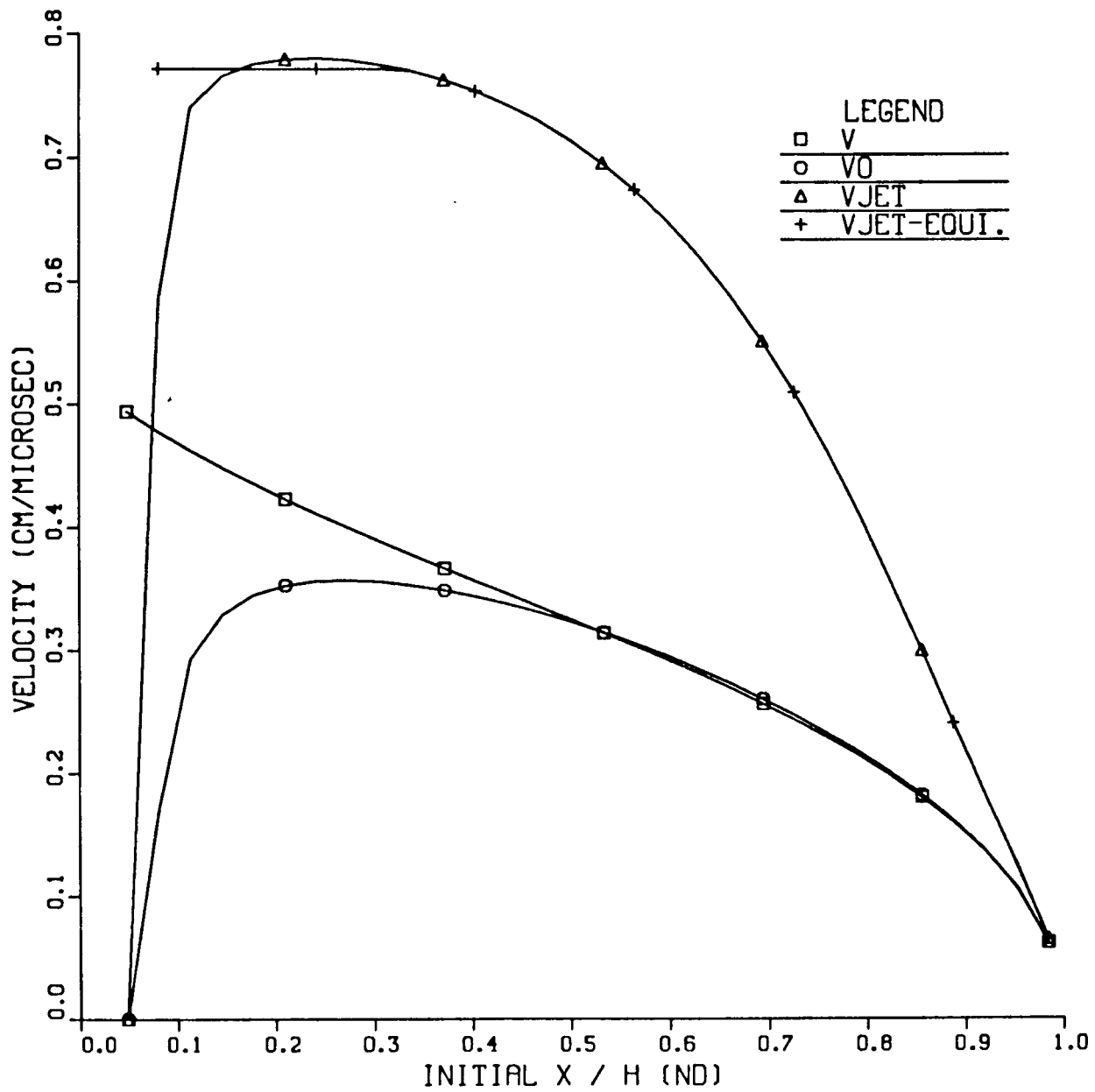
```
DEFAULT = 3 => 1
DEFAULT = 1 => (cr)
Maximum snapshot output time = 0.150E+02 => 30
Maximum snapshot output time = 0.300E+02 => (cr)
Time interval between snapshots = 0.100E+02 => (cr)
Do you wish plotted output? (=Y)
Y (cr)
* SHADING TYPE *
- DENSE = 0
- SPARSE = 1
- NONE = 2

SHADING FLAG = 2 => 1
SHADING FLAG = 1 => (cr)
Do you wish detailed penetration plots
at each and every standoff? (=Y)
(cr)
You can still get one detailed penetration
plot at a single standoff by setting
IPDETAIL equal to a number between
1 and NSOFF = 10
IPDETAIL = 0 => 4
IPDETAIL = 4 => (cr)
Fixed frame size for time snapshots? (=Y)
(cr)
Do you wish hardcopy output? (=Y)
Y (cr)
OUTPUT FILE NAME = DJMS1B.LIS
```

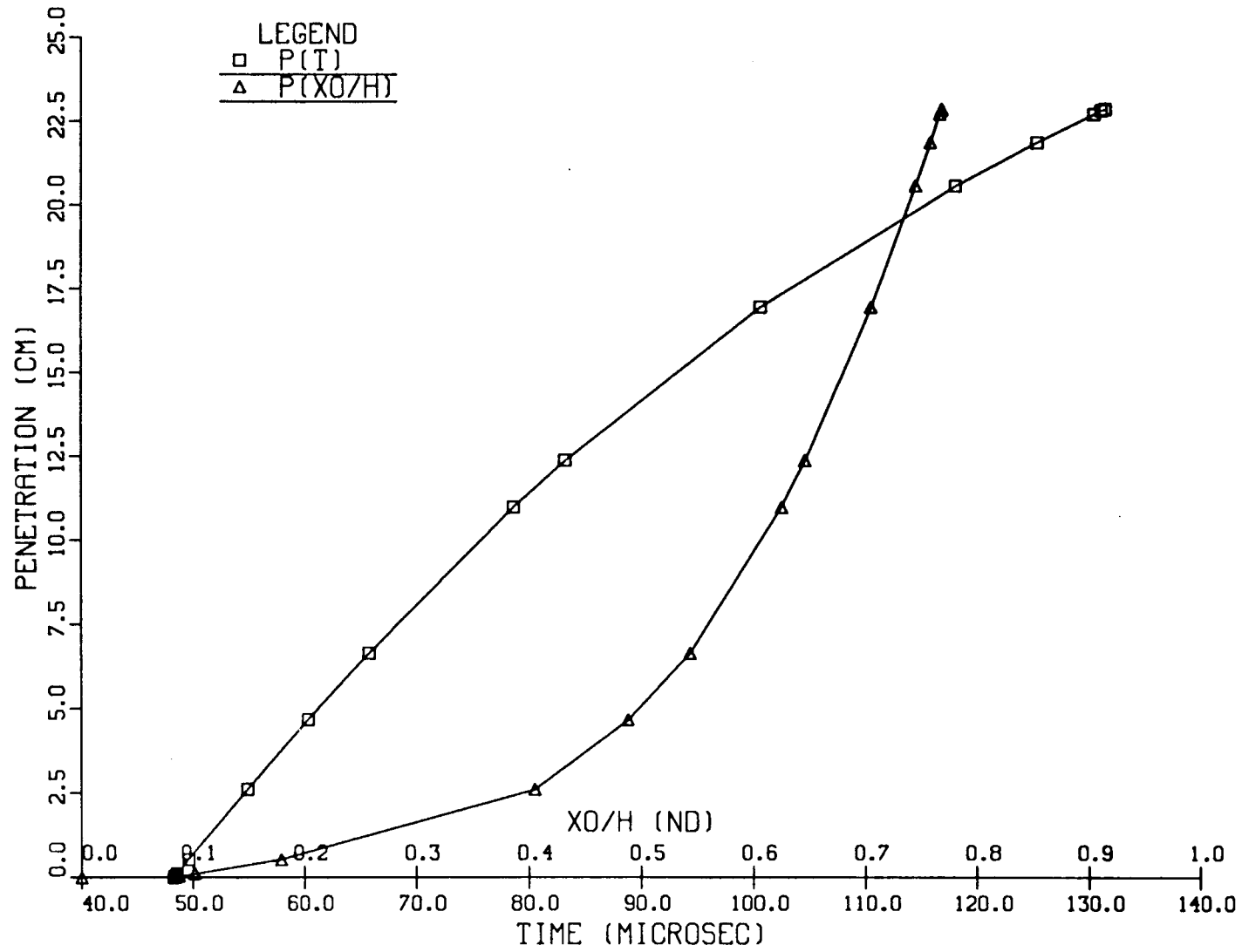
The computation and output will then proceed from this point. On interactive plotting devices, the user must hit a key (e.g. the space bar) to move to the next plot. Otherwise, the plotting output is sent to an appropriate file for further user processing (see Appendix D). Hardcopy output will be found in file DJMS1B.LIS. It may be obtained at a local terminal printer or it may be sent to the system printer using the PRINT command. Pages 61-79 give the plotted output and hardcopy resulting from the input deck and modeling and output options described above.

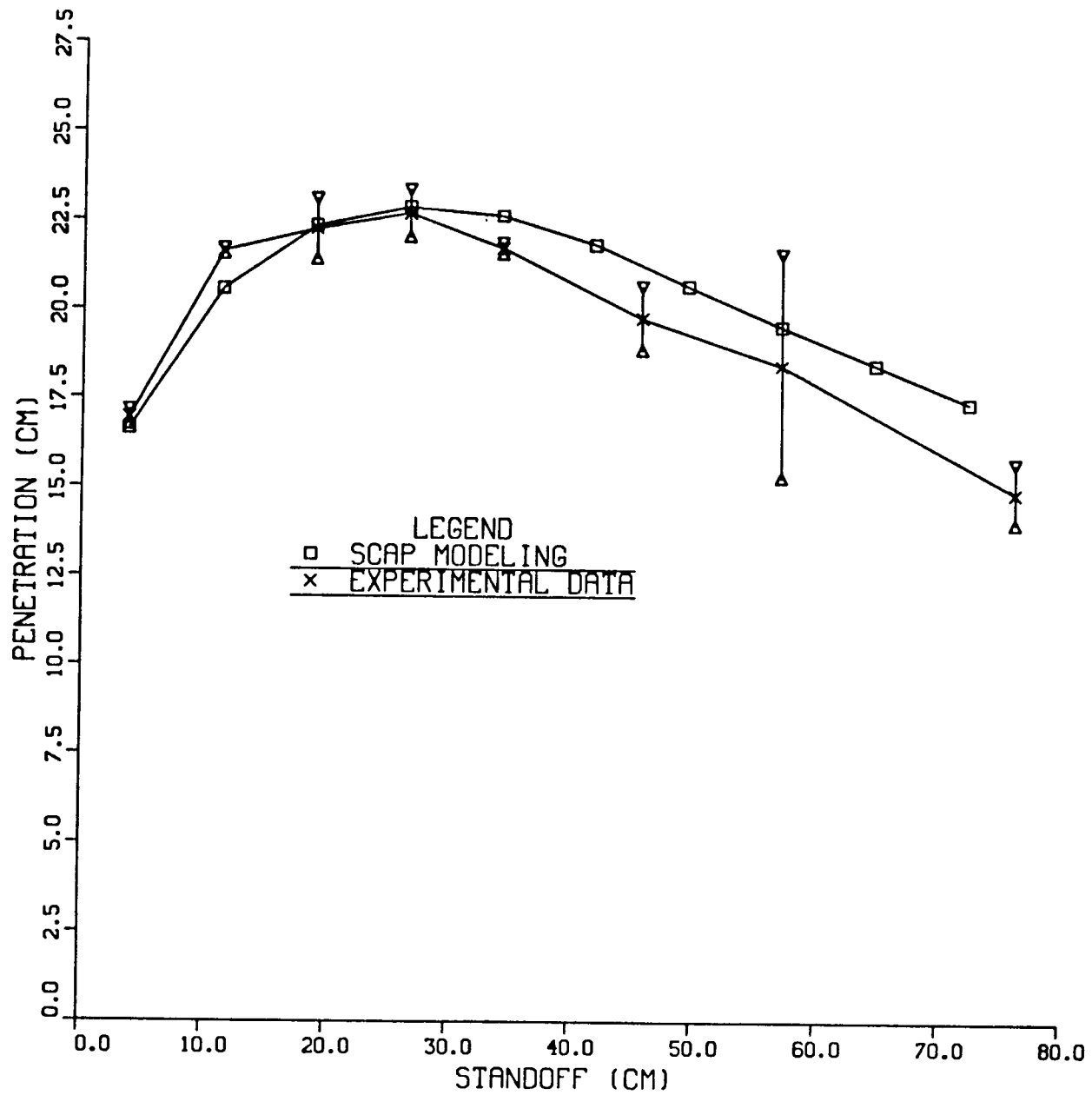


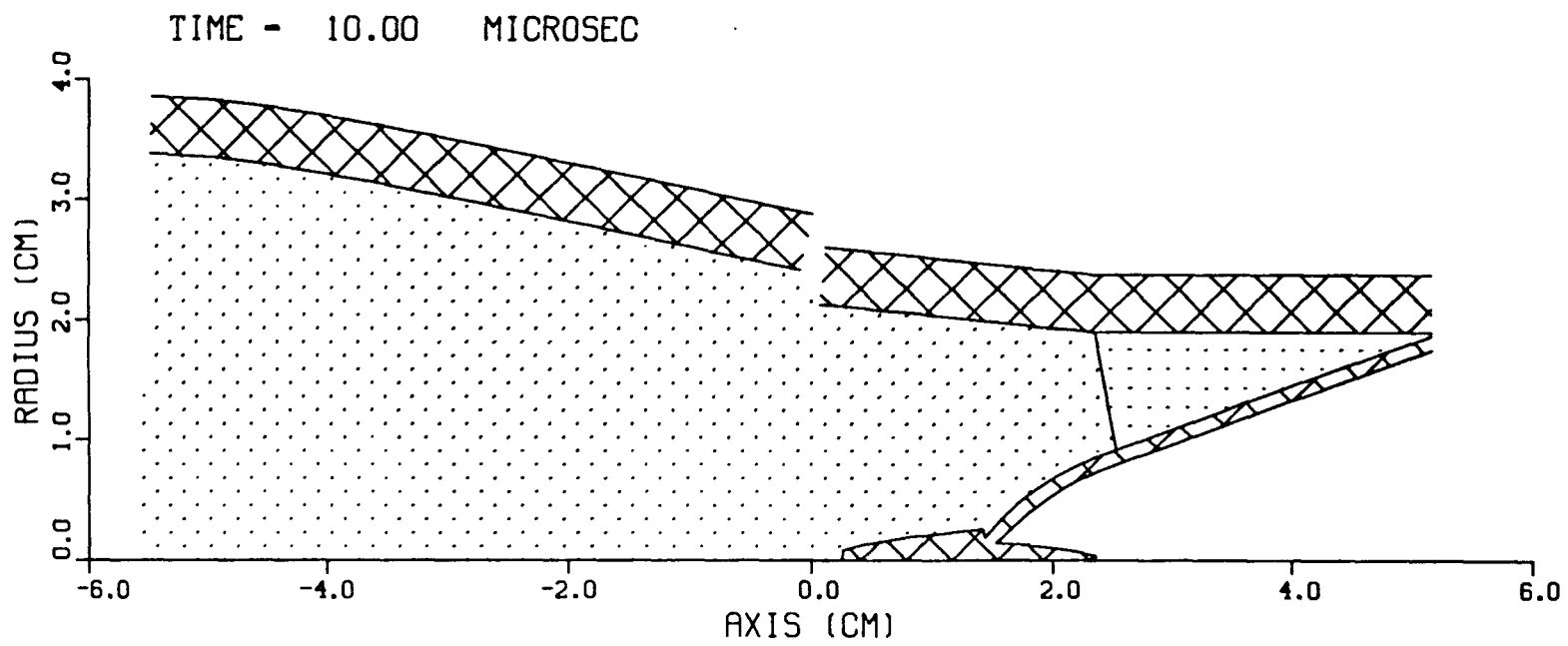




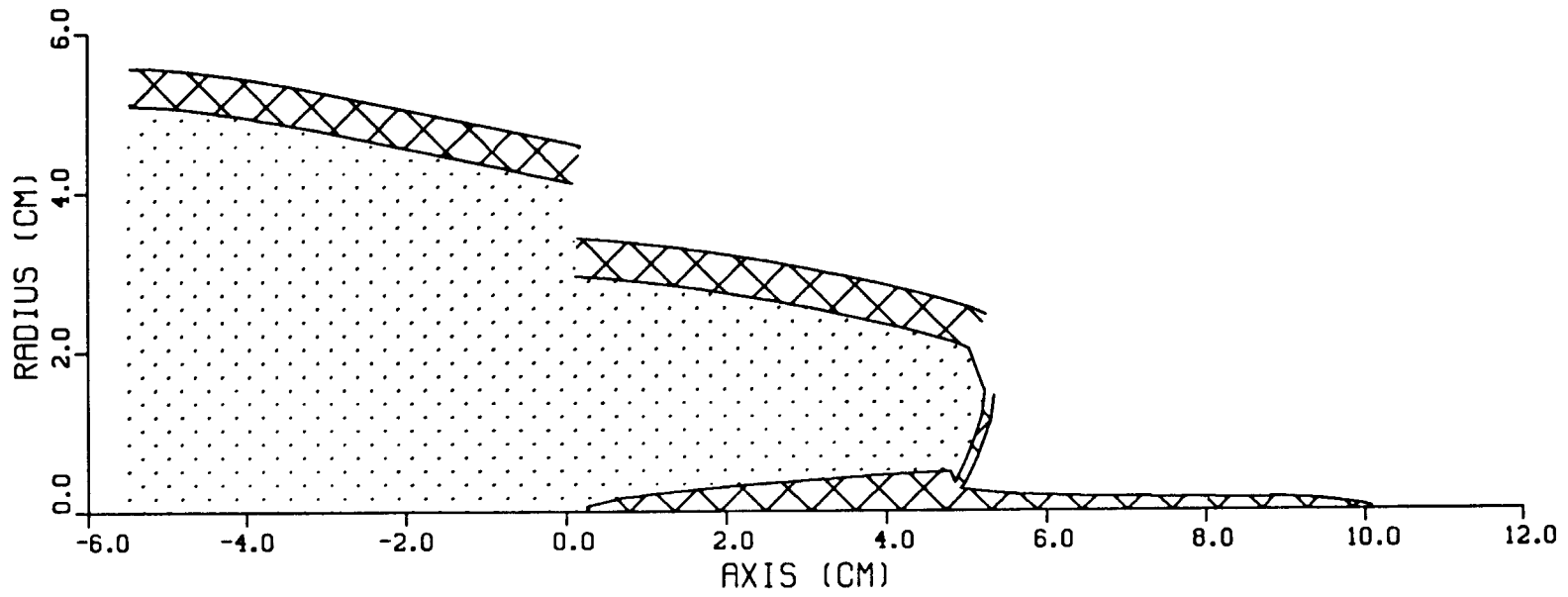
PENETRATION AT 0.267E+02 (CM) STANDOFF

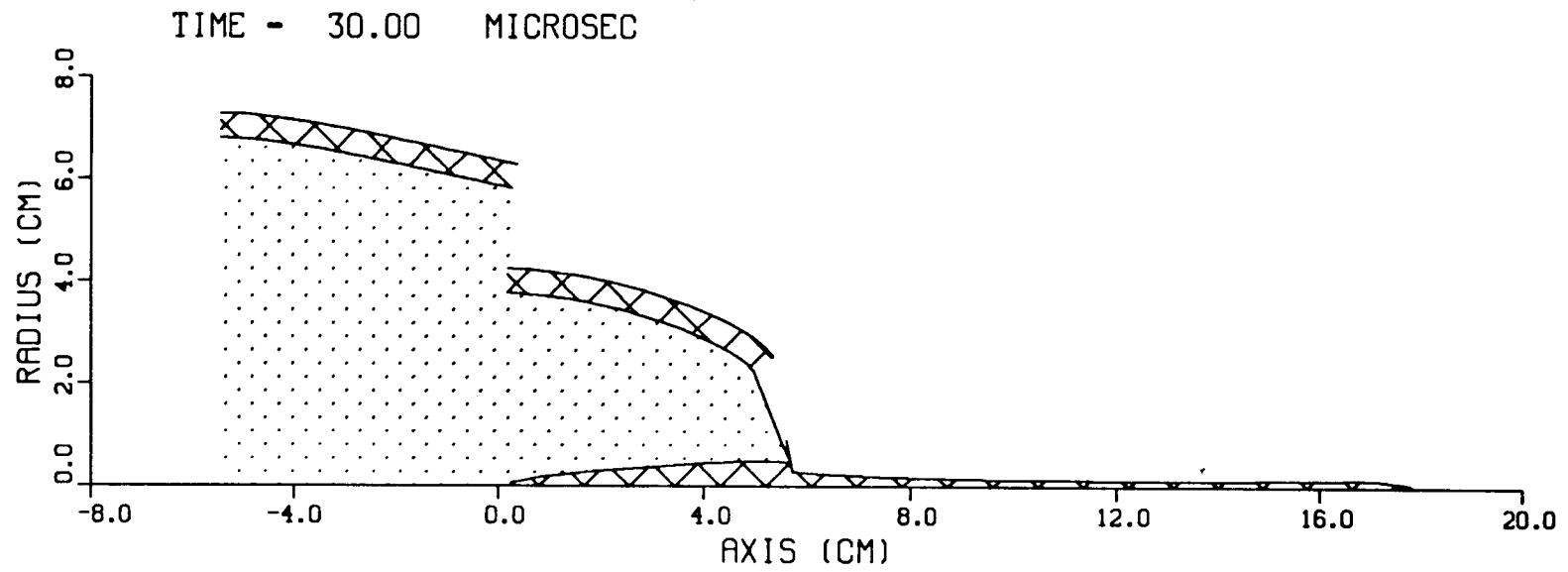






TIME - 20.00 MICROSEC





S C A P

DATE - TIME: 14-MAR-85 - 15:50:54

MODELING CHOICES

IACCEL = 4
 IGURZONE= 1
 IAXIS = 2
 IINTER = 2
 ISIMDET = 1
 IBREAK = 2

INPUT DECK - DJMS1B.DAT THIS FILE - DJMS1B.LIS

MASS LENGTH TIME
 GRAM CM MICROSEC

IGEOM NZ ETYPE DEXP VDET RT2E GAMMA
 2 30 COMP B 0.172E+01 0.798E+00 0.300E+00 0.285E+01

DLIN VBLKL CUTJET TB T1 YLIN NL
 0.894E+01 0.392E+00 0.123E+01 0.000E+00 0.639E+02 0.200E-02 3

LINER PARAMETERS
 0.200E+02 0.178E+01 0.117E+00

DCON NC
 0.785E+01 3
 CONFINEMENT PARAMETERS
 0.000E+00 0.190E+01 0.476E+00

HDET RDET H SOFFMIN SOFFMAX NSOFF NTL
 0.108E+02 0.800E+00 0.523E+01 0.381E+01 0.724E+02 10 1

DTAR THICK UMIN HOLEC
 0.785E+01 0.100E+05 0.160E+00 0.540E+01

CONFINEMENT VELOCITY (XI<0)

XCDDET (CM)	VCON (CM/MICROSEC)
-0.549E+01	0.171E+00
-0.531E+01	0.171E+00
-0.512E+01	0.171E+00
-0.493E+01	0.171E+00
-0.475E+01	0.171E+00
-0.456E+01	0.171E+00
-0.438E+01	0.171E+00
-0.419E+01	0.171E+00
-0.400E+01	0.171E+00
-0.382E+01	0.171E+00
-0.363E+01	0.171E+00
-0.344E+01	0.171E+00
-0.326E+01	0.171E+00
-0.307E+01	0.171E+00
-0.289E+01	0.171E+00
-0.270E+01	0.171E+00
-0.251E+01	0.171E+00
-0.233E+01	0.171E+00
-0.214E+01	0.171E+00
-0.195E+01	0.171E+00
-0.177E+01	0.171E+00
-0.158E+01	0.171E+00
-0.140E+01	0.171E+00
-0.121E+01	0.171E+00
-0.102E+01	0.171E+00
-0.838E+00	0.171E+00
-0.652E+00	0.171E+00
-0.465E+00	0.171E+00
-0.279E+00	0.171E+00
-0.931E-01	0.171E+00

CONFINEMENT VELOCITY (XI>0)

XCDDET (CM)	VCON (CM/MICROSEC)
0.872E-01	0.822E-01
0.262E+00	0.826E-01
0.436E+00	0.829E-01
0.611E+00	0.831E-01
0.785E+00	0.832E-01
0.960E+00	0.831E-01
0.113E+01	0.828E-01
0.131E+01	0.825E-01
0.148E+01	0.820E-01
0.166E+01	0.813E-01
0.183E+01	0.805E-01
0.201E+01	0.796E-01
0.218E+01	0.785E-01
0.236E+01	0.772E-01
0.253E+01	0.758E-01
0.270E+01	0.742E-01
0.288E+01	0.724E-01
0.305E+01	0.704E-01
0.323E+01	0.682E-01
0.340E+01	0.658E-01
0.358E+01	0.631E-01
0.375E+01	0.602E-01
0.393E+01	0.570E-01
0.410E+01	0.534E-01
0.428E+01	0.494E-01
0.445E+01	0.450E-01
0.462E+01	0.398E-01
0.480E+01	0.338E-01
0.497E+01	0.262E-01
0.515E+01	0.151E-01

JET FORMATION OUTPUT

I	XO/H(ND)	VJET (CM/MICROSEC)	DMJET/DLIN (ND)	BETA (DEG)
2	0.810E-01	0.772E+00	0.827E-01	0.334E+02
3	0.113E+00	0.772E+00	0.153E+00	0.461E+02
4	0.145E+00	0.772E+00	0.181E+00	0.503E+02
5	0.178E+00	0.772E+00	0.194E+00	0.523E+02
6	0.210E+00	0.772E+00	0.201E+00	0.533E+02
7	0.242E+00	0.772E+00	0.205E+00	0.539E+02
8	0.274E+00	0.772E+00	0.207E+00	0.541E+02
9	0.307E+00	0.772E+00	0.207E+00	0.542E+02
10	0.339E+00	0.770E+00	0.207E+00	0.541E+02
11	0.371E+00	0.763E+00	0.206E+00	0.540E+02
12	0.403E+00	0.754E+00	0.205E+00	0.538E+02
13	0.436E+00	0.743E+00	0.204E+00	0.536E+02
14	0.468E+00	0.729E+00	0.203E+00	0.535E+02
15	0.500E+00	0.714E+00	0.202E+00	0.534E+02
16	0.532E+00	0.695E+00	0.202E+00	0.534E+02
17	0.565E+00	0.674E+00	0.202E+00	0.535E+02
18	0.597E+00	0.649E+00	0.204E+00	0.537E+02
19	0.629E+00	0.620E+00	0.208E+00	0.542E+02
20	0.661E+00	0.587E+00	0.213E+00	0.550E+02
21	0.694E+00	0.550E+00	0.221E+00	0.561E+02
22	0.726E+00	0.509E+00	0.233E+00	0.578E+02
23	0.758E+00	0.462E+00	0.251E+00	0.601E+02
24	0.790E+00	0.411E+00	0.275E+00	0.633E+02
25	0.823E+00	0.357E+00	0.310E+00	0.676E+02
26	0.855E+00	0.299E+00	0.358E+00	0.735E+02
27	0.887E+00	0.240E+00	0.422E+00	0.811E+02
28	0.919E+00	0.181E+00	0.504E+00	0.905E+02
29	0.952E+00	0.123E+00	0.598E+00	0.101E+03
30	0.984E+00	0.642E-01	0.663E+00	0.109E+03

MASS TOTALS (GRAM)

JET	SLUG	LINER
0.102E+02	0.224E+02	0.326E+02
EXPLOSIVE	CONFINEMENT	
0.178E+03	0.545E+03	

TOTAL JET KINETIC ENERGY (GRAM(CM/MICROSEC)**2)
0.103E+01

JET BREAKUP

I	XAXIS (CM)	TLAXIS (MICROSEC)	TBREAK (MICROSEC)
2	0.428E+00	0.751E+01	0.760E+02
3	0.622E+00	0.799E+01	0.760E+02
4	0.820E+00	0.845E+01	0.760E+02
5	0.102E+01	0.892E+01	0.760E+02
6	0.122E+01	0.939E+01	0.760E+02
7	0.142E+01	0.987E+01	0.760E+02
8	0.162E+01	0.103E+02	0.760E+02
9	0.183E+01	0.108E+02	0.760E+02
10	0.203E+01	0.113E+02	0.760E+02
11	0.223E+01	0.118E+02	0.760E+02
12	0.243E+01	0.123E+02	0.760E+02
13	0.263E+01	0.128E+02	0.760E+02
14	0.283E+01	0.133E+02	0.760E+02
15	0.303E+01	0.138E+02	0.760E+02
16	0.323E+01	0.143E+02	0.760E+02
17	0.343E+01	0.149E+02	0.760E+02
18	0.363E+01	0.155E+02	0.760E+02
19	0.383E+01	0.160E+02	0.760E+02
20	0.403E+01	0.167E+02	0.760E+02
21	0.422E+01	0.173E+02	0.760E+02
22	0.442E+01	0.180E+02	0.760E+02
23	0.461E+01	0.188E+02	0.760E+02
24	0.480E+01	0.197E+02	0.760E+02
25	0.499E+01	0.207E+02	0.760E+02
26	0.517E+01	0.219E+02	0.760E+02
27	0.535E+01	0.235E+02	0.760E+02
28	0.553E+01	0.258E+02	0.760E+02
29	0.569E+01	0.298E+02	0.760E+02
30	0.583E+01	0.422E+02	0.760E+02

LEAST SQUARES VIRTUAL ORIGIN

XVIR (CM)	TVIR (MICROSEC)	CVIR (ND)
0.246E+01	0.121E+02	0.952E+00

PENETRATION OUTPUT AT 0.381E+01 (CM) STANDOFF.

TIME (MICROSEC)	PENETRATION (CM)	INITIAL X / H (ND)
0.187E+02	0.000E+00	0.000E+00
0.187E+02	0.229E-01	0.848E-01
0.190E+02	0.137E+00	0.104E+00
0.205E+02	0.710E+00	0.210E+00
0.255E+02	0.269E+01	0.469E+00
0.302E+02	0.438E+01	0.584E+00
0.361E+02	0.626E+01	0.667E+00
0.536E+02	0.108E+02	0.772E+00
0.710E+02	0.144E+02	0.817E+00
0.774E+02	0.156E+02	0.828E+00
0.829E+02	0.165E+02	0.837E+00
0.836E+02	0.166E+02	0.838E+00
0.842E+02	0.166E+02	0.839E+00

PENETRATION OUTPUT AT 0.114E+02 (CM) STANDOFF.

TIME (MICROSEC)	PENETRATION (CM)	INITIAL X / H (ND)
0.285E+02	0.000E+00	0.000E+00
0.286E+02	0.422E-01	0.880E-01
0.292E+02	0.253E+00	0.125E+00
0.318E+02	0.131E+01	0.318E+00
0.359E+02	0.290E+01	0.452E+00
0.409E+02	0.475E+01	0.546E+00
0.460E+02	0.648E+01	0.607E+00
0.634E+02	0.117E+02	0.713E+00
0.809E+02	0.160E+02	0.764E+00
0.983E+02	0.195E+02	0.798E+00
0.103E+03	0.203E+02	0.805E+00
0.104E+03	0.205E+02	0.807E+00
0.105E+03	0.206E+02	0.808E+00
0.105E+03	0.206E+02	0.808E+00

PENETRATION OUTPUT AT 0.191E+02 (CM) STANDOFF.

TIME (MICROSEC)	PENETRATION (CM)	INITIAL X / H (ND)
0.384E+02	0.000E+00	0.000E+00
0.386E+02	0.615E-01	0.912E-01
0.393E+02	0.369E+00	0.147E+00
0.432E+02	0.190E+01	0.371E+00
0.482E+02	0.382E+01	0.476E+00
0.559E+02	0.658E+01	0.569E+00
0.733E+02	0.122E+02	0.674E+00
0.908E+02	0.168E+02	0.729E+00
0.108E+03	0.204E+02	0.767E+00
0.115E+03	0.217E+02	0.779E+00
0.118E+03	0.221E+02	0.784E+00
0.120E+03	0.224E+02	0.786E+00
0.121E+03	0.224E+02	0.788E+00

PENETRATION OUTPUT AT 0.267E+02 (CM) STANDOFF.

TIME (MICROSEC)	PENETRATION (CM)	INITIAL X / H (ND)
0.483E+02	0.000E+00	0.000E+00
0.483E+02	0.130E-01	0.849E-01
0.484E+02	0.298E-01	0.877E-01
0.486E+02	0.113E+00	0.102E+00
0.496E+02	0.532E+00	0.179E+00
0.549E+02	0.261E+01	0.405E+00
0.603E+02	0.467E+01	0.488E+00
0.657E+02	0.664E+01	0.543E+00
0.787E+02	0.110E+02	0.625E+00
0.832E+02	0.124E+02	0.646E+00
0.101E+03	0.170E+02	0.705E+00
0.118E+03	0.206E+02	0.745E+00
0.125E+03	0.219E+02	0.758E+00
0.130E+03	0.228E+02	0.767E+00
0.131E+03	0.229E+02	0.768E+00
0.131E+03	0.229E+02	0.769E+00

PENETRATION OUTPUT AT 0.343E+02 (CM) STANDOFF.

TIME (MICROSEC)	PENETRATION (CM)	INITIAL X / H (ND)
0.582E+02	0.000E+00	0.000E+00
0.584E+02	0.934E-01	0.966E-01
0.596E+02	0.560E+00	0.182E+00
0.654E+02	0.288E+01	0.407E+00
0.705E+02	0.482E+01	0.475E+00
0.756E+02	0.669E+01	0.523E+00
0.931E+02	0.123E+02	0.626E+00
0.111E+03	0.168E+02	0.687E+00
0.128E+03	0.204E+02	0.729E+00
0.135E+03	0.217E+02	0.743E+00
0.140E+03	0.225E+02	0.752E+00
0.141E+03	0.227E+02	0.753E+00
0.142E+03	0.227E+02	0.755E+00

PENETRATION OUTPUT AT 0.419E+02 (CM) STANDOFF.

TIME (MICROSEC)	PENETRATION (CM)	INITIAL X / H (ND)
0.680E+02	0.000E+00	0.000E+00
0.681E+02	0.205E-01	0.872E-01
0.682E+02	0.465E-01	0.915E-01
0.685E+02	0.177E+00	0.114E+00
0.701E+02	0.827E+00	0.235E+00
0.778E+02	0.383E+01	0.434E+00
0.855E+02	0.661E+01	0.510E+00
0.103E+03	0.120E+02	0.613E+00
0.120E+03	0.163E+02	0.674E+00
0.138E+03	0.198E+02	0.716E+00
0.145E+03	0.211E+02	0.731E+00
0.148E+03	0.215E+02	0.736E+00
0.149E+03	0.217E+02	0.738E+00
0.150E+03	0.218E+02	0.739E+00
0.150E+03	0.219E+02	0.740E+00

PENETRATION OUTPUT AT 0.495E+02 (CM) STANDOFF.

TIME (MICROSEC)	PENETRATION (CM)	INITIAL X / H (ND)
0.779E+02	0.000E+00	0.000E+00
0.780E+02	0.234E-01	0.881E-01
0.781E+02	0.532E-01	0.931E-01
0.784E+02	0.202E+00	0.119E+00
0.803E+02	0.947E+00	0.258E+00
0.878E+02	0.377E+01	0.431E+00
0.954E+02	0.635E+01	0.503E+00
0.113E+03	0.114E+02	0.603E+00
0.130E+03	0.156E+02	0.664E+00
0.148E+03	0.190E+02	0.707E+00
0.156E+03	0.203E+02	0.722E+00
0.158E+03	0.207E+02	0.726E+00
0.159E+03	0.207E+02	0.730E+00

PENETRATION OUTPUT AT 0.572E+02 (CM) STANDOFF.

TIME (MICROSEC)	PENETRATION (CM)	INITIAL X / H (ND)
0.878E+02	0.000E+00	0.000E+00
0.881E+02	0.128E+00	0.103E+00
0.897E+02	0.771E+00	0.222E+00
0.975E+02	0.357E+01	0.424E+00
0.105E+03	0.609E+01	0.496E+00
0.123E+03	0.110E+02	0.595E+00
0.140E+03	0.149E+02	0.656E+00
0.158E+03	0.182E+02	0.698E+00
0.164E+03	0.193E+02	0.711E+00
0.166E+03	0.196E+02	0.713E+00
0.167E+03	0.196E+02	0.717E+00

PENETRATION OUTPUT AT 0.648E+02 (CM) STANDOFF.

TIME (MICROSEC)	PENETRATION (CM)	INITIAL X / H (ND)
0.977E+02	0.000E+00	0.000E+00
0.980E+02	0.139E+00	0.104E+00
0.998E+02	0.836E+00	0.234E+00
0.107E+03	0.349E+01	0.421E+00
0.115E+03	0.586E+01	0.491E+00
0.133E+03	0.105E+02	0.588E+00
0.150E+03	0.143E+02	0.648E+00
0.167E+03	0.176E+02	0.690E+00
0.170E+03	0.180E+02	0.696E+00
0.172E+03	0.183E+02	0.699E+00
0.173E+03	0.185E+02	0.701E+00
0.174E+03	0.185E+02	0.704E+00

PENETRATION OUTPUT AT 0.724E+02 (CM) STANDOFF.

TIME (MICROSEC)	PENETRATION (CM)	INITIAL X / H (ND)
0.108E+03	0.000E+00	0.000E+00
0.108E+03	0.150E+00	0.106E+00
0.110E+03	0.898E+00	0.245E+00
0.116E+03	0.296E+01	0.403E+00
0.120E+03	0.434E+01	0.449E+00
0.125E+03	0.565E+01	0.486E+00
0.134E+03	0.799E+01	0.540E+00
0.142E+03	0.101E+02	0.581E+00
0.160E+03	0.138E+02	0.640E+00
0.177E+03	0.169E+02	0.682E+00
0.180E+03	0.173E+02	0.687E+00
0.180E+03	0.174E+02	0.688E+00
0.181E+03	0.174E+02	0.689E+00

PENETRATION STANDOFF SUMMARY

STANDOFF (CM)	PENETRATION (CM)	COMPLETION TIME (MICROSEC)
0.381E+01	0.166E+02	0.842E+02
0.114E+02	0.206E+02	0.105E+03
0.191E+02	0.224E+02	0.121E+03
0.267E+02	0.229E+02	0.131E+03
0.343E+02	0.227E+02	0.142E+03
0.419E+02	0.219E+02	0.150E+03
0.495E+02	0.207E+02	0.159E+03
0.572E+02	0.196E+02	0.167E+03
0.648E+02	0.185E+02	0.174E+03
0.724E+02	0.174E+02	0.181E+03

JET INFORMATION AT TIME = 0.100E+02 (MICROSEC)

I	XO (CM)	X (CM)	R (CM)
2	0.424E+00	0.235E+01	0.416E-01
3	0.593E+00	0.218E+01	0.762E-01
4	0.762E+00	0.201E+01	0.100E+00
5	0.930E+00	0.185E+01	0.118E+00
6	0.110E+01	0.169E+01	0.132E+00
7	0.127E+01	0.153E+01	0.145E+00

JET INFORMATION AT TIME = 0.200E+02 (MICROSEC)

I	XO (CM)	X (CM)	R (CM)
2	0.424E+00	0.101E+02	0.416E-01
3	0.593E+00	0.989E+01	0.762E-01
4	0.762E+00	0.973E+01	0.100E+00
5	0.930E+00	0.957E+01	0.118E+00
6	0.110E+01	0.941E+01	0.132E+00
7	0.127E+01	0.924E+01	0.145E+00
8	0.144E+01	0.908E+01	0.155E+00
9	0.161E+01	0.891E+01	0.160E+00
10	0.177E+01	0.872E+01	0.155E+00
11	0.194E+01	0.849E+01	0.153E+00
12	0.211E+01	0.825E+01	0.156E+00
13	0.228E+01	0.799E+01	0.159E+00
14	0.245E+01	0.773E+01	0.161E+00
15	0.262E+01	0.745E+01	0.164E+00
16	0.279E+01	0.717E+01	0.167E+00
17	0.296E+01	0.688E+01	0.171E+00
18	0.312E+01	0.658E+01	0.176E+00
19	0.329E+01	0.628E+01	0.182E+00
20	0.346E+01	0.598E+01	0.191E+00
21	0.363E+01	0.569E+01	0.202E+00
22	0.380E+01	0.541E+01	0.219E+00
23	0.397E+01	0.515E+01	0.244E+00
24	0.414E+01	0.492E+01	0.278E+00

JET INFORMATION AT TIME = 0.300E+02 (MICROSEC)

I	XO (CM)	X (CM)	R (CM)
2	0.424E+00	0.178E+02	0.416E-01
3	0.593E+00	0.176E+02	0.762E-01
4	0.762E+00	0.174E+02	0.100E+00
5	0.930E+00	0.173E+02	0.118E+00
6	0.110E+01	0.171E+02	0.132E+00
7	0.127E+01	0.170E+02	0.145E+00
8	0.144E+01	0.168E+02	0.155E+00
9	0.161E+01	0.166E+02	0.156E+00
10	0.177E+01	0.164E+02	0.141E+00
11	0.194E+01	0.161E+02	0.132E+00
12	0.211E+01	0.158E+02	0.132E+00
13	0.228E+01	0.154E+02	0.131E+00
14	0.245E+01	0.150E+02	0.130E+00
15	0.262E+01	0.146E+02	0.129E+00
16	0.279E+01	0.141E+02	0.129E+00
17	0.296E+01	0.136E+02	0.128E+00
18	0.312E+01	0.131E+02	0.128E+00
19	0.329E+01	0.125E+02	0.128E+00
20	0.346E+01	0.119E+02	0.129E+00
21	0.363E+01	0.112E+02	0.131E+00
22	0.380E+01	0.105E+02	0.135E+00
23	0.397E+01	0.978E+01	0.141E+00
24	0.414E+01	0.904E+01	0.150E+00
25	0.431E+01	0.830E+01	0.164E+00
26	0.448E+01	0.758E+01	0.184E+00
27	0.464E+01	0.690E+01	0.211E+00
28	0.481E+01	0.628E+01	0.246E+00
29	0.498E+01	0.571E+01	0.285E+00

After all computations are completed the program continues with

SCAP run completed for input file DJMS1B.DAT

Jet tip velocity = .772 (CM/MICROSEC)

Standoff - Penetration (CM-CM)

3.81	-	16.6
11.4	-	20.6
19.1	-	22.4
26.7	-	22.9
34.3	-	22.7
41.9	-	21.9
49.5	-	20.7
57.2	-	19.6
64.8	-	18.5
72.4	-	17.4

Do you wish to end SCAP modeling session? (=Y)

(cr)

SCAP modeling session will continue.

Input file name = DJMS1B.DAT

In the above case the user chose to continue with the modeling session. The program returned to the beginning with the old file name as the default.

DISTRIBUTION:

U. S. Army Ballistic Research Lab.
Aberdeen Proving Ground, MD 21005

J. T. Harrison
K. Kimsey
F. Grace
S. B. Segletes
W. P. Walters

Joseph Backofen
P. O. Box 1925
Washington, D. C. 20013

Battelle Columbus Lab.
505 King Avenue
Columbus, OH 43201
J. White

Dyna East Corporation
3132 Market Street
Philadelphia, PA 19104
P. C. Chou
R. D. Ciccarelli

Honeywell, Inc.
Defense Systems Division
Hopkins, MN 55343
G. R. Johnson

Lawrence Livermore Lab.
Livermore, CA 94550
M. J. Murphy
M. van Thiel
J. L. Levatin

Los Alamos Scientific Lab.
P. O. Box 1663

Los Alamos, NM 87545
E. H. Farnum
L. Hantell
R. Karpp
J. Walsh

Naval Weapons Center
Materials Engineering Branch
China Lake, CA 93555
G. A. Hayes

Sandia Internal:

331 G. S. Brown
1500 W. Herrmann
1510 J. W. Nunziato
1511 G. G. Weigand
1512 J. C. Cummings
1513 D. W. Larsen
1520 D. J. McCloskey
1521 R. D. Krieg
1522 R. C. Reuter
1523 J. H. Biffle
1524 W. N. Sullivan
1524 D. B. Longcope
1530 L. W. Davison
1531 S. L. Thompson
1531 T. J. Burns
1531 J. W. Swegle
1531 F. J. Zeigler
1533 P. Yarrington
1533 M. E. Kipp
1533 A. C. Robinson (25)
1534 J. R. Asay
1540 W. C. Luth
1601 J. L. Dossey
2510 D. H. Anderson

2512 J. G. Harlan
2512 M. G. Vigil
2513 J. E. Kennedy
2513 P. L. Stanton
2514 B. H. Van Domelen
2514 S. R. Kurowski
2515 P. D. Wilcox
2567 S. Skolnick
3141 C. M. Ostrander (5)
3151 W. L. Garner (3)
3154-3 C. Dalin (28) For DOE/TIC
5341 M. J. Forrestal
7132 P. W. Cooper
8430 L. D. Bertholf
8024 M. A. Pound